UNDERSTANDING IONIC TRANSPORT IN THE MACROSTRUCTURE OF POLYSACCHARIDE BOUND ELECTRODES FOR CAPACITIVE DEIONIZATION

BY

MARTINA DEL CERRO

THESIS

Submitted in partial fulfillment of the requirements
for the degree of Master of Science in Environmental Engineering in Civil Engineering
in the Graduate College of the
University of Illinois at Urbana-Champaign, 2018

Urbana, Illinois

Adviser:

Assistant Professor Roland D. Cusick

ABSTRACT

Capacitive deionization (CDI) is increasingly being considered as a promising desalination alternative to reverse osmosis and other well-established technologies, especially when it comes to treating low salinity water, such as groundwater. Lifetime and charge efficiency (CE) are the two metrics which determine the competitiveness of CDI technologies, which is why enhancing design is a major developmental challenge. It is known that ion-exchange membranes (IEMs) and chemical surface modification contribute to this goal by eliminating the effects of co-ion repulsion. Previous research conducted in our lab, showed how the use of charged biodegradable polysaccharide compounds, namely chitosan (CS) and carboxymethylcellulose (CMC), as anodic and cathodic electrode binders respectively, improved charge efficiency and lifetime values of the electrodes in which they were employed, compared to a symmetric cell where electrodes were bound with the traditionally used, petrochemically derived, polyvinylidene fluoride (PVDF). As a means of comparison, surface-modified electrodes were also fabricated and their performance assessed when assembling them in another CDI unit. The specific salt adsorption (SSA) behavior of the CS-CMC bound cell, combined with the cyclic voltammetry (CV) results and SSA at various discharge voltages, suggested the binder was enhancing salt adsorption performance and mitigating co-ion repulsion by modifying the macrostructure, producing a similar effect to an IEM.

In this work, we propose a mechanism for the enhanced salt adsorption and charge efficiency observed with the charged polysaccharide binders, where a hybrid system composed of CDI and MCDI sub-units can illustrate the effects of the improved electrode macrostructure. We fit the untreated carbon data using the Amphoteric Donnan Model (ADM) to consider the

asymmetry in acidic and basic groups in the pristine carbon surface, which is the main cause of co-ion repulsion. The SSA value calculated for this system only differs by 5% from that obtained experimentally and charge efficiency shows a similar trend. To simulate impact of charged binders on ionic transport within the electrode macropores, MCDI sub-units were introduced. At a MCDI surface coverage of 7.5% we observe the co-ion repulsion peak disappears as a result of the addition of fixed charge. When decreasing the membrane thickness, thus resembling the polysaccharide coating of the carbon, the diffusion timescale across the selective interface is significantly reduced, and therefore governs the overall cell behavior by modifying the concentration in the flow channel for subsequent units. The model discretizes rapid transport across these selective interfaces and slower transport across traditional CDI sub-units, although in reality the electrode structure is much more complex and thus differences between the simulated results and the actual behavior can find reason in this simplification. Finally, we determine that an anode binder pKa should be one log unit greater than the influent pH to make the system less sensitive to pH fluctuations.

DEDICATION

I dedicate this work to my family who have supported me unconditionally in every decision I have made throughout my life, and to my friends in the USA, who have been my unconditional family for the past two years.

ACKNOWLEDGEMENTS

A special thanks to my advisor Roland Cusick whose guidance, support and trust made me not only become a better professional but also a better person, by presenting me with challenges that made me realize my full potential. To the Fulbright Commission for making this experience possible. And to my lab group colleagues, without whom my working experience would not have been as enjoyable.

TABLE OF CONTENTS

CHAPTER 1

INTRODUCTION

The World Health Organization estimated in 2017 that 844 million people in the world, that is one out of ten, did not have access to clean water (Joint Monitoring Program Report 2017). Richard Smalley (Rice University) lists water as the second main problem humanity will face during the next 50 years, right below energy. Given that there is more brackish than freshwater in the world, making desalination technologies more energy and cost effective is a promising area of research. Among the most widely employed desalination technologies, distillation, reverse osmosis and electrodialysis can be highlighted (Porada et al., 2013). Although effective for their purpose, they require high energy inputs. Capacitive deionization (CDI) has received increasing amounts of attention when it comes to treating water with a salinity content below 10 g/L due to its low energy consumption, and its potential for energy re-use.

In CDI cells, the water stream flows through/between two porous, typically carbonaceous electrodes, which upon polarization induce the electromigration of ions and their adsorption in electrical double layers (EDLs). After some time, the electrodes become saturated, and the cell is discharged, releasing a brine stream which can be used, under certain operating conditions, to generate an electric current and recycle this energy.

The two metrics that determine the potential for scalability of CDI technologies are charge efficiency and lifetime. Employing ion exchange membranes (IEMs) and modifying the chemical surface charge of the electrodes have been two of the most widely employed methods for improving selectivity and charge efficiency (Suss et al., 2015; Gao et al., 2012). Placing

membranes in front of the electrodes blocks co-ions from being released into the solution upon polarization of the cell. Ideally, one ion salt molecule will be removed from the solution per electron transferred between the electrodes, contrary to what happens in traditional CDI, where less than one salt molecule will be adsorbed per electron transferred. This effect increases the charge efficiency of the desalination process. Additionally, if the cell is discharged with reverse polarity, membranes can enhance the depletion of the electrode, hence restoring its capacity for the next desalination step (Biesheuvel & Van der Wal, 2010). Membranes typically consist of a polymeric backbone which has ions adhered to it: negatively charged groups in the case of cation exchange membranes (CEM) and positively charged groups in the case of anion exchange membranes (AEM). These groups constitute "nondiffusible fixed charges", and according to the Donnan exclusion principle they control the distribution of ions in the membrane and in the phase adjacent to it (Sarkar & Sengupta, 2010), through the creation of an equilibrium potential (Xu, 2005). Surface modified carbons expand the voltage operating window of the electrodes by shifting the potential of zero charge (PZC). Provided this parameter corresponds to the polarization value at which the electrode will exhibit minimum capacitance, the electrode's counter-ion adsorption capacity is improved while leaving the charge necessary to achieve it unchanged. These phenomena lead to increased CE values, as well as higher SSAs.

Although effective, these methods increase the systems cost due to the high prices of IEMs (Yan et al., 2018) and the resource intensity of carbon surface modification. Therefore, there is a clear need for alternatives that achieve the same objectives while being more economical if CDI is operation is to be positioned in the operative region where it can become competitive with RO, for example (Figure 1) (Hand et al., in prep.). Polysaccharide binders such as CS and CMC provide an economically and environmentally feasible alternative given that

their employment does not suppose the use of organic solvents, and are comparatively cheap to IEMs and reactants used for carbon modification. Recent work in our lab has shown how the incorporation of these biodegradable binders increased CE and SSA almost three times compared to a cell bound with PVDF, rendering them a viable alternative for enhancing performance.

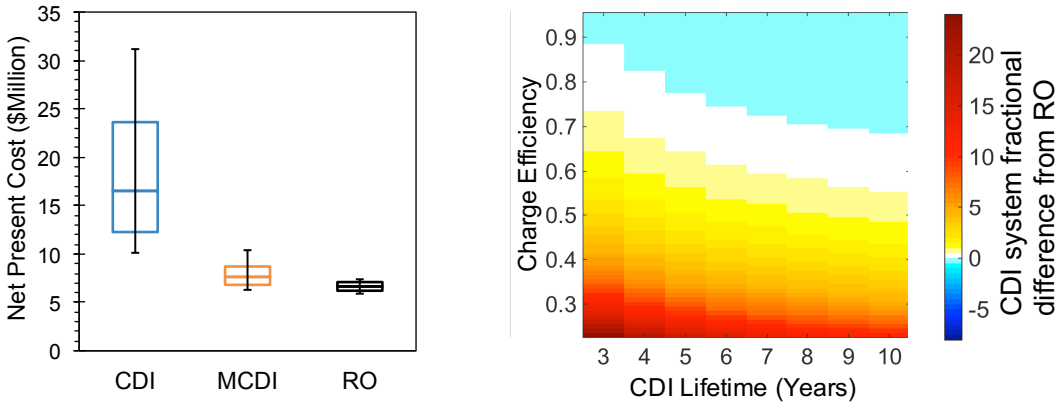

Figure 1. Estimative comparison between CDI, MCDI and RO (Hand et al., in prep.). It is concluded that for CDI technologies to become economically viable at a large scale, lifetime and charge efficiency need to be in the area shaded blue in Figure b.

Understanding the principles that govern the CDI process is as important as finding materials that are suitable for the cells operation. Recent work on molecular dynamics for example, has shown how the nanostructure can play a fundamental role when determining the passage of water molecules or ions (Zhang et al., 2017). It is therefore evident, how applying a mechanistic approach can reduce the randomness of trial and error when employing new materials or designing new cell architectures. Several models have been developed over the years to explain the adsorption process in porous carbon electrodes (Hemmatifar et al., 2015). The latest are based on the Donnan theory, where electrical double layers are highly overlapped and so the potential can be assumed to be constant inside the electrode micropores, where adsorption

takes place (Biesheuvel et al., 2011). A recent modification of the Donnan model accounted for fixed chemical charge on the carbon surface, which is normally assumed to be perfectly balanced (Biesheuvel, 2015). In this work, we advance the understanding of ionic flux in electrode macropores when binders with fixed charge are used, by proposing a mechanism through which the polysaccharide binders enhance CDI performance. We introduce asymmetry in the fixed chemical charge to assess the impacts of this imbalance in SSA and CE, and assess the binders' impacts on the macrostructure by simulating transport with an intercalation of CDI and MCDI sub-cells. We fit the data of the as-received carbon system bound with PVDF, carbon bound with polysaccharides as well as surface modified carbon electrodes, concluding with a suggestion to leverage the potential of charged polysaccharide bound electrodes to make the system insensitive to pH fluctuations.

CHAPTER 2

LITERATURE REVIEW

2.1 Current and Future Challenges of the Water-Energy Nexus

Current exponential population growth comes associated with a consequent increase in resource consumption, specifically energy and water. As populations continue to grow and prosper economically, the energy consumption per capita increases. Energy production requires water, and similarly, water services require energy. Withdrawals of water destined to power plant cooling, fuel extraction and processing surpass all those of any other industry in the United States, while the water sector consumes 12.6% of all energy production (Tidwell, 2016). Also, as a result of climate change, water supplies are projected to decline (National Climate Assessment, 2014), and it is expected that by 2025, 3.5 billion people in the world will live under water-stressed conditions (Service, 2006). The major flaw in policy making regarding these two resources is that they are usually treated independently of one another, which introduces vulnerabilities as the limitations in one sector have direct consequences in the other (Stillwell et al., 2011). The 2011 drought in Texas, is illustrative of all these points: 100 days of temperature above 100°F resulted in record electricity demand and reservoir levels below what had been experienced historically (Scanlon et al., 2013).

A systemic approach is therefore needed to develop policies, processes and analytical tools that contemplate the interdependencies between the two sectors. In the water sector, conservation efforts have increased and major improvements have been made on infrastructure, but these measures only serve for optimizing use, rather than increasing supply; which is why

desalination and reuse seem like sensible solutions to ensure freshwater availability (Elimelech & Phillip, 2011). However, when breaking down the total cost of produced water, energy accounts for around 50% of the total cost (Al-Karaghouli & Kazmerski, 2013), thus shedding light on the fact that energy optimization in water desalination technologies is a potential ground for innovation.

2.2 Overview of Desalination Technologies

2.2.1 Distillation

Distillation is one of the oldest desalination processes and makes use of thermal energy to separate water from the dissolved ions, based on the fact that water is volatile, and ions are not. The two most common types of distillation processes are multi-effect distillation (MED) multi-stage flash distillation (MSF). In MED, heat is transferred from steam condensation to the feed solution in a series of effects (Van der Bruggen & Vandecasteele, 2002). The main problems encountered when using this technology is scaling of the surfaces as accumulation of salt creates heat transfer resistances with time which make the process more energy intensive (Table 1), and corrosion. MSF is mainly used for seawater desalination and consists of a "series of flash chambers where steam is generated from seawater at a progressively reduced pressure", and later on condensed. 50% of the world's desalination water production is obtained through this technique in the Persian Gulf (Semiat, 2008). One of the main advantages of MSF as opposed to MED, is that scaling does not occur, as heat is not transferred through conducting surfaces, and its relative operation simplicity.

Table 1. Comparison of the total capacity and energy consumption of different desalination sources (Al-Karaghouli and Kazmerski, 2013).

Property	MSF	MED	SWRO	BWRO	ED
Capacity (m^3/d)	50 k – 70 k	5 k – 15 k	Up to 128 k	Up to 98 k	2 – 145 k
Total electricity consumption (kWh/m^3)	19.58 – 27.25	14.45 – 21.35	4 - 6	1.5 – 2.5	2.64 – 5.5 0.7 – 2.5 at low TDS
Product quality (ppm)	~10	~10	400 - 500	200 - 500	150 - 500

2.2.2 Reverse osmosis

Reverse osmosis (RO) is a desalination process which employs pressures higher than the osmotic pressure of the feed solution, to enable water passage through a semi-permeable membrane, leaving ions behind in what is called the concentrate. There are two branches in reverse osmosis operation: sea water (SWFO) and brackish water (BWFO) desalination. The two differ mainly in the kind of pretreatment required, the applied pressures and the kind of fouling they are prone to (Greenlee et al., 2009). The greatest improvements in efficiency have been achieved through membrane design optimization (Peng Lee et al., 2011) and energy recovery systems connected in line with the concentrate (Ghaffour et al., 2013). Reverse osmosis is highly versatile in terms of the water salinity and feed water composition, obtaining high production rates and efficiencies, which makes this technology the most widely used nowadays for desalination (Figure 2). The drawbacks associated with this technology include membrane fouling, which brings the necessity of adding a pre-treatment phase before subjecting the membrane to the feed water.

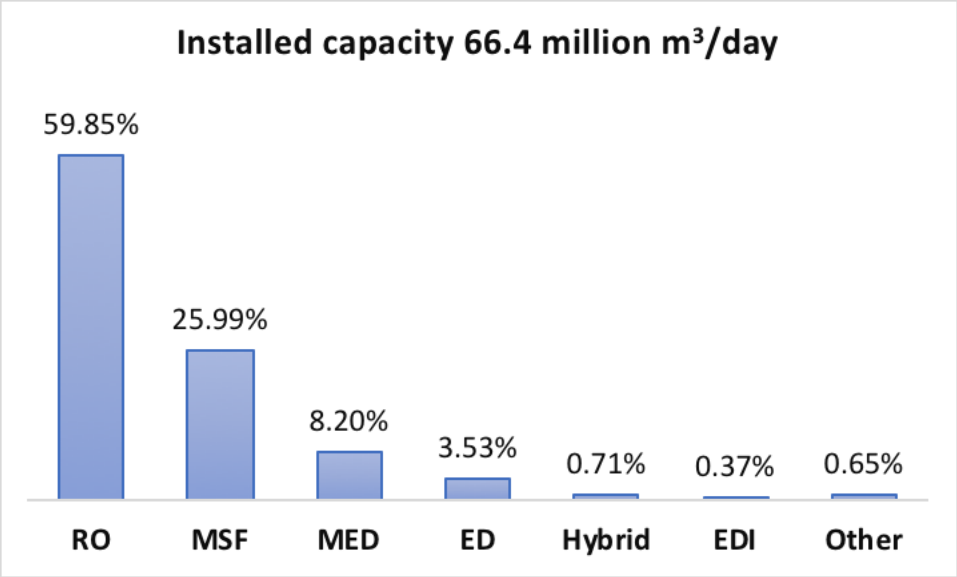

Figure 2. Breakdown of the total capacity of installed thermal and membrane processes in 2012 (Ghaffour et al., 2013).

2.2.3 Electrodialysis

Electrodialysis (ED) is a separation process based on ion transport through ion exchange membranes induced by applying an electric field. It is mainly used for desalination from brackish water sources, typically in small to medium sized plants (Strathmann, 2010). Most ED devices are composed of a stack of parallel IEMs, to achieve higher removals. ED is mainly used for treating brackish water, since its advantages can only be leveraged with a certain feed water composition (Strathmann, Stuttgart University). The main drawback of electrodialysis is that uncharged species are not removed from the feed, and for high salinity waters the energy consumption is too high to be competitive with other alternatives, although it is at salt concentrations up to 3000 ppm (Fritzmann et al., 2006). Also, as in every process that employs membranes, they are subject to scaling and fouling.

Variations of this technology include Reverse Electrodialysis (RED) used to mix two different water streams with different concentration, with the goal of obtaining energy (Veerman

& Vermaas, 2016). While ED uses electrical energy with a separation goal, RED generates electricity.

2.3 Capacitive Deionization technologies

Capacitive deionization has existed since the 1960s. It has recently received lots of attention, due to its low energy consumption and high achievable efficiencies when treating brackish and surface waters (Oren, 2008). Under certain operation conditions, it is also possible to recover energy (Długołęcki, & van der Wal, 2013). Desalination occurs when polarizing a set of porous carbon electrodes, where ions are adsorbed and stored in EDLs. An overview is given in order to understand the current state of the technology, and gaps for potential development.

2.3.1 CDI performance metrics

To publish advancements in the technology development, the CDI community has agreed on establishing the following metrics as performance assessment parameters (Suss et al., 2015):

- *Salt adsorption capacity (SAC) or most recently, salt specific adsorption (SSA) [mg/g]*: mass of salt removed from feed water divided by the electrode mass.
- *Average salt adsorption rate (ASAR) [mg/g/s]*: Provides information on the rate of salt adsorption. The convention is to divide the total salt mass removed by the total electrode mass (both anode and cathode added) and the total adsorption/desorption cycling time.
- *Kim-Yoon diagrams:* Plot of ASAR vs SSA. These plots help determine the optimal point of operation, which will result from the maximum product of both parameters. They also illustrate under which operating conditions the system is mass-transfer or reaction rate limited.

- *Charge storage capacity:* Corresponds to the total amount of charge the system can store, and it is simply the conversion of salt adsorbed to Coulombs.
- *Charge efficiency:* Ratio of adsorbed salt over charge applied. It is one of the most important metrics when rendering these technologies scalable and competitive.

2.3.2 CDI cell architectures

2.3.2.1 Flow-by and flow-through CDI

The most traditional CDI cell is the "flow-by" cell (FB CD) which consists of two parallel carbon electrodes separated by a spacer, where the feed solution flows in between the electrodes in the axial direction (Suss et al., 2015). Typical CE values for CDI cells are 0.5-0.8 (Kim et al., 2015). Flow-through electrode capacitive desalination (FTE CD) was later on incorporated since it was proved that the charging process occurred more rapidly if the feed solution went through the electrodes, i.e. flowing in their normal direction, aligned with the electric field (Avraham et al., 2009). This architecture reduces both the desalination time (4-10 times higher than FB CD) and can desalinate feed with higher concentration per charge (Suss et al., 2012). The system's resistance is reduced as well by eliminating the need for a separator. The major limitation in designing these electrodes comes from finding a material that is porous enough to allow the fluid to be transported without the need of a high pressure gradient, while still having a high microporosity to exhibit high salt storage, which is why research efforts have been focusing on developing hierarchical structures that reunite all desired characteristics (Zhao et al., 2016).

2.3.2.2 Membrane Capacitive Deionization (MCDI)

A big leap was made in CDI performance with the addition of IEMs to the cell: an anion exchange membrane in front of the anode, and a cation exchange membrane in front of the cathode. Incorporation of membranes has shown to increase salt removal by 20% compared to CDI (Biesheuvel et al., 2011), as well as charge efficiency (Zhao et al., 2012). The amount by which these two metrics are improved is dependent upon several factors, among which the AR-C characteristics, influent salt concentration, operation parameters can be distinguished, but in general, CE in MCDI can be four times higher than in CDI (Zhao et al., 2013). The reasons behind the increase in performance are that membranes provide charge selectivity and mitigate parasitic current due to co-ion repulsion (Suss et al., 2015) and by blocking the passage of co-ions, the macropores in the carbon serve as additional storage space (Tian et al., 2014). They also represent a physical barrier to oxygen reaching the cathode (Tang et al., 2017), which is known to unleash a series of Faradaic reactions which produce the oxidation of the anode and a progressively decaying performance of the cells. IEMs have also been added in the form of coatings on the carbon surfaces, given that this approach diminishes the system's resistances (Porada et al., 2013). Specific capacitance has been reported to increase by up to 30% when employing coated membranes (Kim & Choi, 2010). A recent work, also illustrated the effects of coating the electrodes with a polyelectrolyte layer (Ahualli et al., 2017), acting as a selective barrier at the flow channel, electrode interface. Although resistance indeed decreased in this system, the mechanistic approach presented aligns well to the experimental data up to a certain point, after which experiment and theory diverge.

IEMs have also been introduced as electrode binders (Jain et al., 2018), reaching CE values around 90% and SSAs of 14 mg/g compared to 5-13 mg/g observed in conventional CDI.

The potential for these crosslinked PVA-bound electrodes had already been realized previously (Park & Choi, 2010), where the specific capacitance was shown to increase compared to hydrophobic PVDF-bound electrodes due to increased wettability.

2.3.2.3 Flow electrodes

The next major modification in CDI cells came with the incorporation of flow electrodes, where a slurry of carbon particles is employed instead of having them in a compacted manner. The main advantages of using flow electrodes is that the cell does not require a discharge step and its potential for scalability given its continuous nature (Jeon et al., 2012). In flow electrode capacitive deionization (FCDI) the electrodes have infinite ion adsorption capacity, and the supplied energy can be recovered up to 20% using an external circuit when operating the system under constant current (Jeon et al., 2014).

2.3.2.4 Inverted CDI

A system where the anode possessed net negative charges and conversely, the cathode possessed net positive charges was fabricated and an opposite behavior to normal CDI operation was observed in this inverted CDI cell (i-CDI) (Gao et al., 2014). This operation increased lifetime values up to 530% compared to a traditional CDI system, due to the reduction in the anode's feasibility for oxidation.

2.3.3 Introduction of polysaccharide compounds as electrode binders

Fabrication of electrodes requires binders that hold the active material and conductive additives, providing stability and adhesion to the current collector. Poly-vinylidene fluoride

(PVDF) is the most widely used polymer for binding activated carbon particles but is high in cost and requires organic solvents to be incorporated into the active material matrix (Chai et al., 2013). CS and CMC had been used effectively in Li-ion batteries improving Coulombic efficiency and cycling stability (Chai et al., 2013; Li et al., 2007). In addition to the increased performance, these binders possess the advantage that they are soluble in innocuous substances for the environment, namely, water and acetic acid.

Work conducted previously (Kim et al., in prep), assembled an asymmetric CDI cell, where the anode was bound with CS and the cathode with CMC; a system referred to as CS-CMC. The system's performance was compared to a cell assembled with electrodes made with as-received carbon (AR-C) and bound with PVDF, a system denoted AR-PVDF, and a surface modified carbon cell, which employed an aminated anode (Am) and an oxidized (Ox) cathode, whose denomination was Am-Ox. Desalination experiments and charge efficiencies calculations showed considerable improvements in the polysaccharide bound system compared to AR-PVDF (Figure 3a & 3b), although the mechanisms for salt adsorption differed from the ones both the AR-PVDF and Am-Ox systems exhibited (Figure 3c). The CS-CMC system did not shift the electrode's PZC, but it did shift the operating voltage window, suggesting the binder was increasing the electrosorption capacity of macropores (Figures 4a & 4b). However, a decrease in performance was observed when changing the influent pH, and thus inducing the deprotonation of CS and loss of fixed charge in the anode, pointing towards the need of a binder with a higher pKa than CS to realize the full potential of the employment of charged binders.

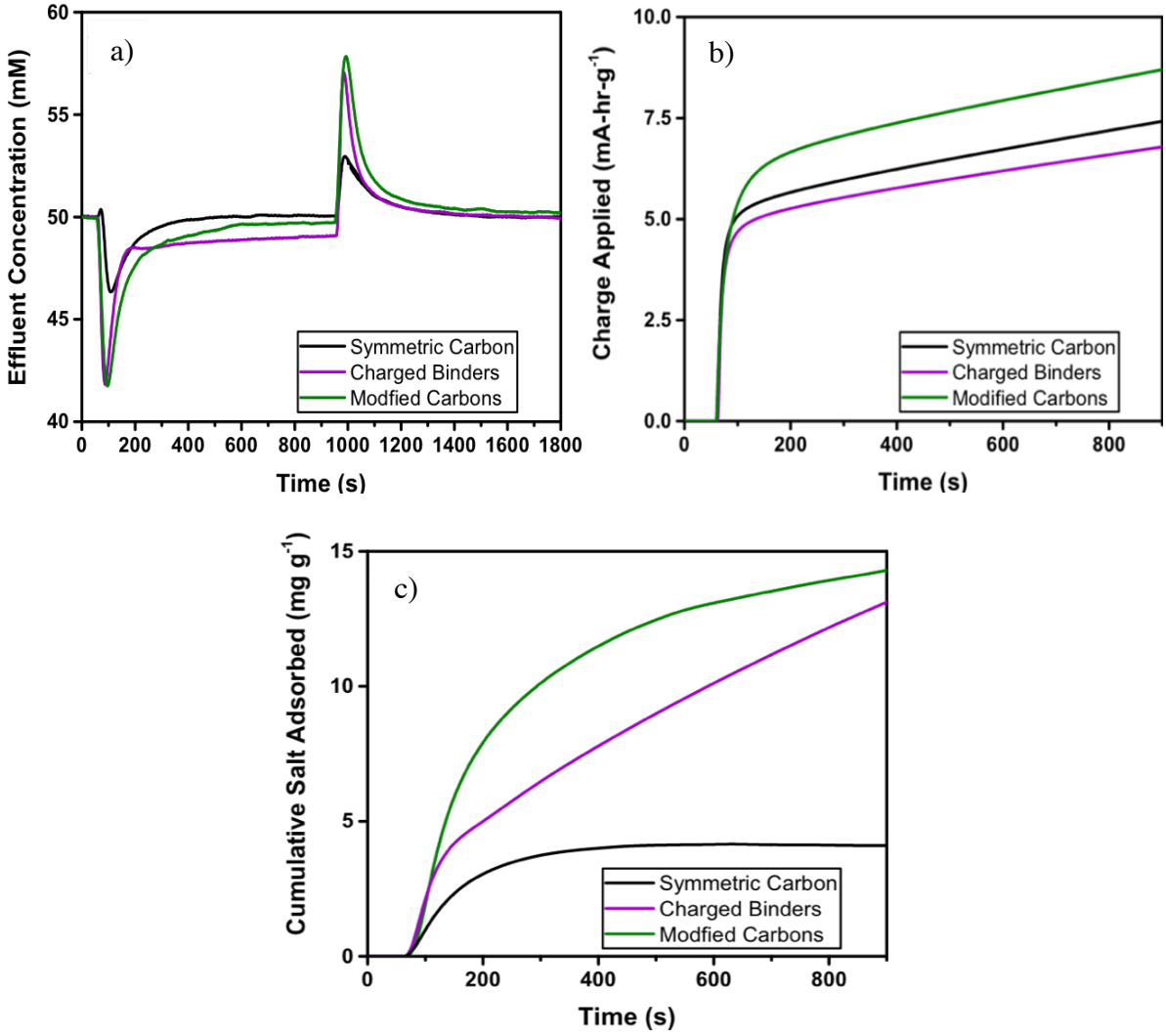

Figure 3. (Kim et al., in prep.) (a) Desalination cycles for AR-PVDF, CS-CMC and Am-Ox systems. (b) Comparison of charge applied to each of the configurations. (c) Comparison between cumulative salt adsorption. The linear part of the binder system reflects MCDI behavior.

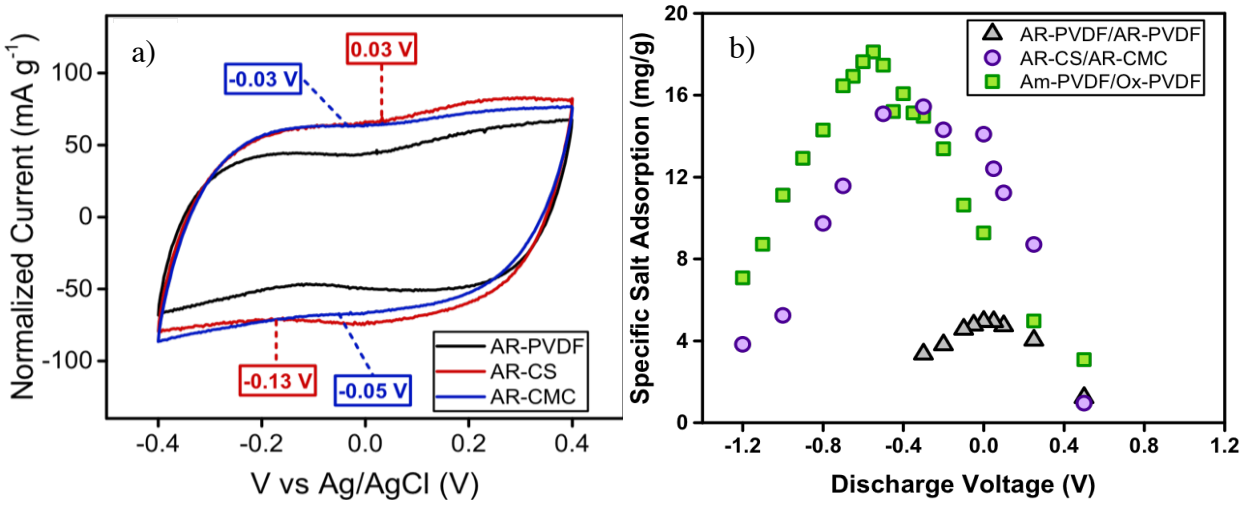

Figure 4. (Kim et al., in prep.) (a) PZC analysis of binder system and AR-PVDF. The CS-CMC system increases capacitance while preserving the AR-C PZC. (b) Variation of the discharge voltage between the different systems. The CS-CMC cell shifted the discharge voltage while preserving PZC, an indication that the macropores adsorption capacity is enhanced.

2.3.4 Constant current vs constant voltage operation

CDI cells can be either operated by applying a constant voltage (CV) during a fixed cycle time or a constant current (CC) which is reverted once the electrode reaches a certain potential. CV operation has an initial high adsorption rate due to the strong initial applied potential gradient, which decreases gradually as the electrodes become saturated. In CV operation the voltage is low in the beginning, and thus SSA is slow and increases linearly with time as the cell voltage increases (Kang et al., 2014). CC mode can produce a more constant ion concentration in the desalinated stream (Zhao et al., 2012), and it also consumes less energy than CV operation, for there is less dissipation of energy through resistive components (Qu et al., 2016) and the time the cell spends at voltages prone to unleash Faradaic currents can be controlled. Finally, one of the main differences between the two operation modes is the possibility of recovering energy in CC operation. Up to 83% energy recovery was achieved in an MCDI cell when operating under CC conditions (Długołęcki, & van der Wal, 2013).

2.3.5 Adsorption models for porous electrodes

Understanding the principles that govern adsorption is complementary to designing new cell architectures and employing new material approaches to enhance the technology performance. Following, a summary of the theory evolution in CDI is presented.

2.3.5.1 Helmholtz theory

The simplest model for ion adsorption on a polarized surface is the Helmoltz model. In this model, the surface charge on the electrode is compensated by a plane containing equal number of charges from the electrolyte but of opposite sign (Figure 5a). This inner Helmholtz plane is located at a distance d from the surface, equal to the radius of the ionic species. The potential drop exhibits a linear behavior with distance and thus it predicts a constant capacitance value (Bard & Faulkner, 2000). This model would predict CE values in CDI systems equal to unity, which is certainly not aligned with the values below 100% efficiency obtained experimentally (Suss et al., 2015).

2.3.5.2 Gouy-Chapman model

Gouy and Chapman (GC) later proposed a model where a diffuse layer was formed adjacent to the electrode surface, given that due to Brownian motion and the attraction/repellent effects of surface polarization a considerable thickness in solution may be needed to counterbalance the electronic charge. The ionic density would be the greatest close to the electrode surface, and decrease with increasing distance from the solid. This suggests that the capacitance is not constant but rather a result of the potential and concentration, which in turn affects the distance ions will be found from the surface. The potential in this model exhibits an

exponential decay instead of a linear one (Figure 5b). However, this model fails to predict experimental systems accurately, by overestimating the capacitance and by assuming the ions in the electrolyte are point charges (Zhang & Zhao, 2009).

2.3.5.3 Gouy-Chapman-Stern model

To account for the fact that ions have indeed a finite size and therefore, cannot approach the surface at a distance smaller than their ionic radius, Stern introduced a modification in GC model leading to the formulation of the Gouy-Chapman-Stern (GCS) model. This modification is the inclusion of the Outer Helmholtz Plane (OHP), regarded as the plane of "closest approach", which is especially important at large polarizations and high electrolyte concentrations, when the system behavior starts resembling Helmholtz's approach. The capacitance is comprised of two serial contributions: i) a Helmholtz or compact layer capacitance where the potential drop is linear, and ii) a diffuse layer capacitance that varies in a V-shaped fashion (Figure 5c) (Bard & Faulkner, 2000; Zhang & Zhao, 2009).

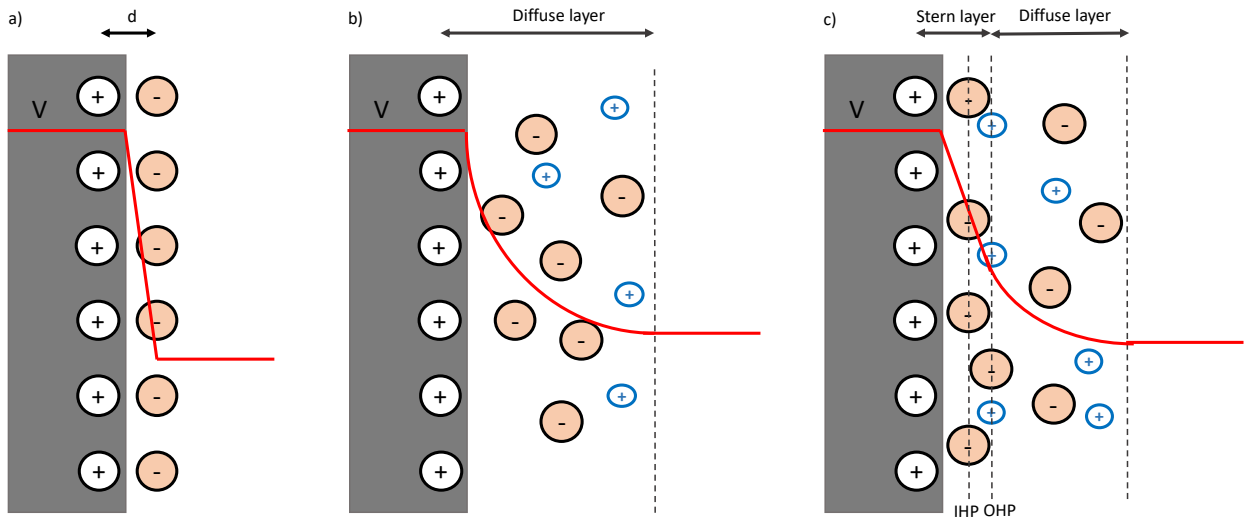

Figure 5. Representation of the different EDL adsorption models. (a) Helmholtz model, (b) GC model, (c) GCS model.

2.3.5.4 Donnan model

The principle behind Donnan equilibrium establishes that potential differences arise on interfaces when charge is selectively being exchanged, and that these potential differences can be calculated from electrochemical potentials (Bard and Faulkner, 2000).

The GCS model proved to be successful in describing equilibrium data for porous electrodes; however, when attempting to model transport, the model fails due to the assumption that the diffuse layer is several orders of magnitude greater than the Debye length (Porada et al., 2012). In the carbon electrodes used for CDI, it has been proven that micropores (less than 2 nm in diameter) are responsible for achieving high desalination capacity (Biesheuvel et al., 2014). In these micropores, diffuse layers are strongly overlapped, and therefore it is valid to make the Donnan assumption that the electrolyte inside the carbon particles has a constant electrical potential (Figure 6).

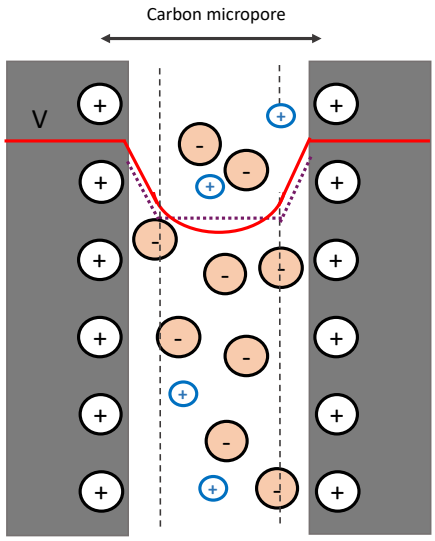

Figure 6. Modified Donnan model (Biesheuvel et al., 2014). It can be seen that in the case of constrained environments, such as a carbon micropore, the EDLs overlap strongly, and thus the potential can be assumed to be constant (dotted purple line).

2.3.5.5 Modified-Donnan model

However, due to the existence of adsorption when the carbon was not polarized, a modified Donnan (m-Donnan) model was proposed, introducing a chemical attraction energy for the ion when it transfers from outside to inside the carbon particles, which is necessary to obtain a better fit of the theory to the experimental data (Guyes et al., 2017). This term is a "non-electrostatic attraction of the ion into the micropores" (Porada et al., 2012).

2.3.5.6 Amphoteric Donnan model (ADM)

To explain adsorption under no polarization conditions as well as to depict CDI behavior when the electrodes surface is chemically modified, the amphoteric Donnan model (ADM) was introduced, representing in a more accurate way than the mD model, the data on the carbon surface characteristics (Biesheuvel, 2015). Two micro-regions are differentiated: acidic and basic, which exhibit opposite polarity, since negative charges on the carbon surface may exist as

a result of carboxylic groups, whereas basic groups may exist due to aminated groups or carbon basal planes proton adsorption (Boehm, 1994). In this model, a charge balance inside the micropores is incorporated, in which the electronic, ionic and chemical charge are perfectly balanced in both regions (Gao et al., 2016).

Although these models have been successful in accurately depicting CDI operation, the behavior observed when introducing polysaccharide binders could not be accurately explained. It is therefore evident that constant innovation in electrode design requires broadening of the scope of current CDI models.

CHAPTER 3

METHODS

3.1 Modeling approach

3.1.1 General considerations and assumptions

To model the different carbon-binder electrode configurations, the cell was divided into sub-cells and a stirred tanks-in-series model used to simulate the fluid dynamics each stirred tank (section 3.2.6, Figure 1). At the end of every cell a transport equation was used to account for the fact that the conductivity measurements are made some time after the effluent has left the cell, and some mixing may occur during this process. The number of units was determined by varying this parameter until obtaining a good fit to the experimental data. The accuracy of the fit was determined by calculating both the SSA and CE of the experimental and modeled curves. To model adsorption, the ADM model was used to account for fixed charge in the carbon micropores.

Several assumptions hold for all the systems analyzed, namely:

- Cathode and anode are symmetric in terms of their mass, porosity and fixed charge
- The electrolyte is symmetric, and the ionic species have equal ionic diffusivities
- Flow channel and electrodes are well-mixed volumes
- The Ohmic resistance is negligible compared to the ionic resistance
- There is a fixed leakage current which has been determined experimentally and held constant throughout the simulations

- No other species are generated from the Faradaic reactions taking place
- When more than one cell was added in series, the leakage current measured from the experiments is distributed proportional to the projected area each sub-cell possesses.
- pH is assumed to be constant throughout the operation, and equivalent to the influent pH set in the experiments.
- IEM's have been assumed to possess the same fixed charge and to be equally pH dependent, thus avoiding the complexity that asymmetric salt adsorption would imply.

Simulations were carried out using COMSOL Multiphysics 5.3 software. For modeling each desalination unit, a General Form PDE interface was employed.

3.1.2 Equilibrium

The main implication of modeling CDI equilibrium accurately is the correct prediction of a co-ion repulsion peak, for it is the adsorption characteristics of the carbon at equilibrium that determine the amount of ionic charge that is stored without the passing of current. In this state, the Donnan and Stern potential are equal in magnitude, and so is the current in both anode and cathode. The system of equations is completed by establishing the ADM charge balance in the micropores. In the expressions that follow, *A* will refer to anode and *C* to cathode.

Since the electrodes are not polarized the following relationship holds:

$$0 = E_A - E_C$$

Where, E_i corresponds to the voltage value of each electrode.

The above expression translates into:

$$0 = \Delta\phi_{DON,A} + \Delta\phi_{ST,A} - \left(\Delta\phi_{DON,C} + \Delta\phi_{ST,C}\right)$$

$\Delta\phi_{DON,i}$ and $\Delta\phi_{ST,i}$ are the Donnan and Stern potentials of each electrode, which can be defined as:

$$\Delta\phi_{ST,i} = \frac{\sigma_{elec,i}\, F}{C_s V_t}$$

$$\Delta\phi_{DON,i} = -asinh\left(\frac{\sigma_{ionic,i}}{2\, C_{ma}}\right)$$

In the micropores, the ADM model establishes that:

$$\sigma_{elec,i} + \sigma_{ionic,i} + \sigma_{chem,i} = 0 \quad (1)$$

In equation 1, $\sigma_{elec,i}$, $\sigma_{ionic,i}$ and $\sigma_{chem,i}$ are the electronic, ionic and fixed chemical charge densities inside the micropores.

There should be no current flow at equilibrium, therefore:

$$m_A\, p_{mi,A}\, \sigma_{elec,A} + m_C\, p_{mi,C}\, \sigma_{elec,C} = 0$$

$m_i\, p_{mi,i}$ makes reference to the mass times the microporosity of the electrode.

The relationship between both regions was established by understanding that the potential drop across the electrical double layer in both regions needs to be the same (Dykstra et al., 2017):

$$\Delta\phi_{DON,A} + \Delta\phi_{ST,A} = \Delta\phi_{DON,B} + \Delta\phi_{ST,B} \quad (2)$$

3.1.3 AR-PVDF cell simulation

The untreated carbon was simulated considering the fixed charge asymmetry on its surface: an imbalance in acidic and basic groups, which is most commonly neglected in ADM models due to the complexity added to the system when introducing more unknown variables. The fixed charge imbalance on the carbon surface however, is the main cause of co-ion repulsion

and its accurate representation contributes significantly to understanding the desalination performance of CDI cells.

The CDI sub-units where modeled as follows:

For the flow channel, Nernst-Planck equations for Sodium and Chloride were added to arrive to a global concentration, potential independent equation (Newman & Thomas-Alyea, 2004) that was discretized following the well-mixed volumes assumption:

$$p_{FC}\frac{dC_{FC}}{dt} = \frac{QC_{in} - QC_{FC}}{V_{FC}} + \frac{D_{eff}}{L_{dif}^2}(C_{ma} - C_{FC})$$

The change in concentration inside the electrode can be calculated by equating the temporal variation of the macropore and micropore concentration to the incoming ionic flux:

$$p_{MA}\frac{dC_{AN}}{dt} + p_{MI}\frac{1}{2}\left(\frac{dC_{MI,A}}{dt} + \frac{dC_{MI,B}}{dt}\right) = -\frac{D_{eff}}{L_{dif}^2}(C_{ma} - C_{FC})$$

The ionic current was calculated by substracting Nernst-Planck equations under the assumption of equal ionic diffusivities and averaging it over the flow channel volume. The following current continuity equation was employed, introducing a fixed value for the leakage current, which was determined from the current vs time curves obtained experimentally:

$$p_{MI}\frac{1}{2}\left(\frac{d\sigma_{elec,A}}{dt} + \frac{d\sigma_{elec,B}}{dt}\right) = (I_{ionic} + I_{leak})\frac{1}{L_{elec}} \qquad , \qquad I_{ionic} = -2\,D_{eff}C_{FC}\frac{\Delta\phi_{ch}}{L_{ch}}F$$

The potential drop across the flow channel was calculated from the total cell voltage equation:

$$-\frac{V_{cell}}{V_t} + 2\,x\left(\Delta\phi_{DON,A} + \Delta\phi_{ST,A}\right) = \Delta\phi_{ch}$$

The model is completed by using equations (1) and (2) for the electrodes, considering both acidic and basic regions.

Finally, at the end of the cell transport in the tubing from the effluent port of the CDI cell to the conductivity meter was modeled according to:

$$\frac{\partial C_{meas}}{\partial t} = vel\ \frac{\partial Cmeas}{\partial x} - D_{FC}\frac{\partial^2 C_{meas}}{\partial x^2}$$

$$vel = \frac{Q}{A_{flux}}, A_{flux} = \frac{\pi\, D_{tube}^2}{4}$$

Equation which was solved considering that the fluid travels through a 7 cm tube before reaching the conductivity probe.

3.1.4 CS-CMC cell simulation

To understand the impacts of introducing the charged polysaccharide binders in the macrostructure, the cell was modeled employing a series of MCDI and CDI sub-units. The equations presented in 3.1.3 still hold for the CDI sub-units, while the MCDI fractions were modeled as follows:

For the flow channel, the ionic fluxes continuity leads to:

$$p_{FC}\frac{dC_{FC}}{dt} = \frac{QC_{in} - QC_{FC}}{V_{FC}} + \frac{D_M}{L_m^2}[(C_{M2} - C_{M1}) - M\,\Delta\phi_M]$$

Where the second term on the right is the distance averaged ionic flux across the membrane (Tedesco et al., 2016), which being rate limiting determines the rate of transport to and from the electrodes.

The concentrations *on the solution side* at the membrane-solution interface and at the membrane-electrode interface with their corresponding Donnan potential drops were calculated according to (Tedesco et. al, 2016):

$$C_{M2} = \sqrt{M^2 + 4C_{ma}^2} \quad , \quad \Delta\phi_{D,m2} = \sinh^{-1}\frac{\pm M}{2C_{ma}}$$

$$C_{M1} = \sqrt{M^2 + 4C_{FC}^2} \quad , \quad \Delta\phi_{D,m1} = \sinh^{-1}\frac{\pm M}{2C_{FC}}$$

M corresponds to the membrane's fixed charge and will be positive in the case of an AEM and negative for a CEM.

The electrode concentration changes develop according to:

$$p_{MA}\frac{dC_{AN}}{dt}+p_{MI}\frac{1}{2}\left(\frac{dC_{MI,A}}{dt}+\frac{dC_{MI,B}}{dt}\right)=-\frac{D_M}{L_m^2}\left[(C_{M2}-C_{M1})-M\,\Delta\phi_M\right]$$

The current conservation equation in this case is:

$$p_{MI}\frac{1}{2}\left(\frac{d\sigma_{elec,A}}{dt}+\frac{d\sigma_{elec,B}}{dt}\right)=(I_{ionic}+I_{leak})\frac{1}{F\,L_{elec}}$$

While the potential drop across the membrane ($\Delta\phi_M$) can be obtained through the cell potential equation which leads to:

$$\Delta\phi_M=\frac{\frac{V_{cell}}{V_t}-2\,(\Delta\phi_{DON,A}+\Delta\phi_{ST,A})-2\,(\Delta\phi_{DON,M2}-\Delta\phi_{DON,M1})}{(2+k)}$$

The ionic current was calculated under the assumption that the concentration in the membrane is approximately equal to the fixed charge. Although this consideration is only valid for ideal membranes and we are indeed solving for interfacial concentrations, the assumption simplifies the number of variables considerably:

$$I_{ionic}=D_m\,M\,\frac{\Delta\phi_M}{L_m}$$

The parameter *k* in the total cell voltage expression comes from the current continuity between the flow channel and the membranes, and helps relate the potential drop across each domain:

$$I_{memb}=I_{FC}\quad,\quad D_m\,M\,\frac{\Delta\phi_M}{L_m}=2\,D_{eff}C_{FC}\frac{\Delta\phi_{ch}}{L_{ch}}F$$

$$k=\frac{D_m\,M\,L_{FC}}{2\,D_{eff}\,C_{FC}\,L_m}$$

The system is completed by making use of equations (1) and (2) to model adsorption in the electrodes.

The parameters used in the model can be visualized in Table 2.

Table 2. Parameters used in the simulations

Parameter	Value [unit]	Description	Calculation
$\boldsymbol{\sigma_{chem,A}}$	-0.26 [mol/l]	Fixed chemical charge of acidic regions	Fitted
$\boldsymbol{\sigma_{chem,B}}$	0.01 [mol/l]	Fixed chemical charge of basic regions	Fitted
$\boldsymbol{C_s}$	85 [F/ml]	Stern layer capacitance	Fitted
$\boldsymbol{D_m}$	0.01 D_{eff}	Diffusion coefficient across the binder layer	Dykstra et al., 2017
$\boldsymbol{D_{eff}}$	$D_{FC}\ p_{FC}^{1.5}$	Effective ionic diffusivity	Bruggeman correction
$\boldsymbol{D_{FC}}$	1.68 x 10^{-5} [m^2/s]	Ionic diffusivity	Guyes et al. 2015
$\boldsymbol{\rho_{elec}}$	0.4664 [g/ml]	Electrode density	Shang et al., 2017
$\boldsymbol{I_{leak}}$	-0.01097 [mA]	Leakage current	Current vs time experiments
$\boldsymbol{M}$	0.6 - 2 [mol/L]	Binder fixed charge	Equilibrium expression fitted
$\boldsymbol{L_{dif}}$	1.2 L_{FC}	Characteristic length of transport from flow channel to the electrodes	Fitted
$\boldsymbol{L_{elec}}$	300 [um]	Electrode depth	Measured
$\boldsymbol{Q}$	0.2 [ml/min]	Flow rate	Fixed
$\boldsymbol{D_{tube}}$	0.5 [mm]	Tube diameter	Measured
$\boldsymbol{L_m}$	15 - 150 [um]	Thickness of binder layer	Fitted
$\boldsymbol{A_{sup}}$	150 [mm^2]	Electrodes surface area	Measured
$\boldsymbol{p_{ma}}$	0.35	Electrode macroporosity	Shang et al., 2017
$\boldsymbol{p_{mi}}$	0.25	Electrode microporosity	Shang et al., 2017
$\boldsymbol{p_{FC}}$	0.7	Flow channel porosity	Shang et al., 2017
$\boldsymbol{rho}$	0.4664 [g/cm^3]	Electrode density	Shang et al., 2017
$\boldsymbol{V_{cell}}$	1.2 [V]	Cell voltage	Fixed

3.1.5 Am-Ox cell

The Am-ox cell was not modeled in this occasion given that the Boehm titration revealed an asymmetry in the fixed charge present in anode and cathode. This would lead to an asymmetric ionic distribution, where ionic species would need to be tracked individually, and Faradaic reactions taking place in the cell would need to be considered, as well as the influent pH. The complexity embedded in this study is not justified for the analysis, provided the novelty of this work arises from the use of charged binders. An approximate description of this system could be achieved however, if an average fixed charge concentration which is equal in magnitude but opposite in polarity is assumed for the anode and cathode. However, these models have been extensively studied and published (Gao et al., 2016; Biesheuvel, 2015) and therefore, a simplified model describing the experimental curve would not add any significant value to this study.

CHAPTER 4

RESULTS AND DISCUSSION

4.1 AR-PVDF modeling

For the AR-C cell, it was possible to model the behavior achieving only an 8% error in the total salt adsorption capacity (Figure 7a), using a single CDI cell (Figure 7b). During the charging step, we achieve to observe a co-ion repulsion peak, product of a 0.25 mol/L imbalance between acidic and basic regions in the AR-C, which is consistent with the results obtained from the Boehm titrations performed in the lab in the background experiments; the only difference being that acidic groups surpass basic groups, which would be the case of a carbon that has undergone oxidation. Provided we are modeling a system which is symmetric from the anode's perspective, the choice was made considering that an anode with fixed negative charge will release co-ions when first polarized. We observe it disappear faster in the simulated system, which may be a product that in the model we are not including a mixing area at the beginning of the cell, and faster diffusion processes may occur at this position, given that the concentration gradient at this point is the highest. The driving force for mass transport is the difference in chemical potentials, which in this case we can relate to concentration given the dilute nature of the system. According to Fick's law, the greater the difference in concentration, the greater the flux, and thus, at the inlet where one differential volume into the cell the concentration has dropped significantly as a result of polarization, and one differential volume outside the cell the concentration is still at C_0 the flux in the axial direction will be the greatest, for this concentration difference between differential volumes is also the greatest that evolves in the cell.

Hence, the extended period and highest value of the co-ion repulsion peak observed in the experiment as opposed to the simulations, may have to do with the fact that the average concentration at the inlet is has this diffusive flux contribution that we are not accounting for. The most accurate approach would have been a Danckwert's kind boundary condition, but we chose to reduce the fitting parameters by using a Dirichlet boundary condition.

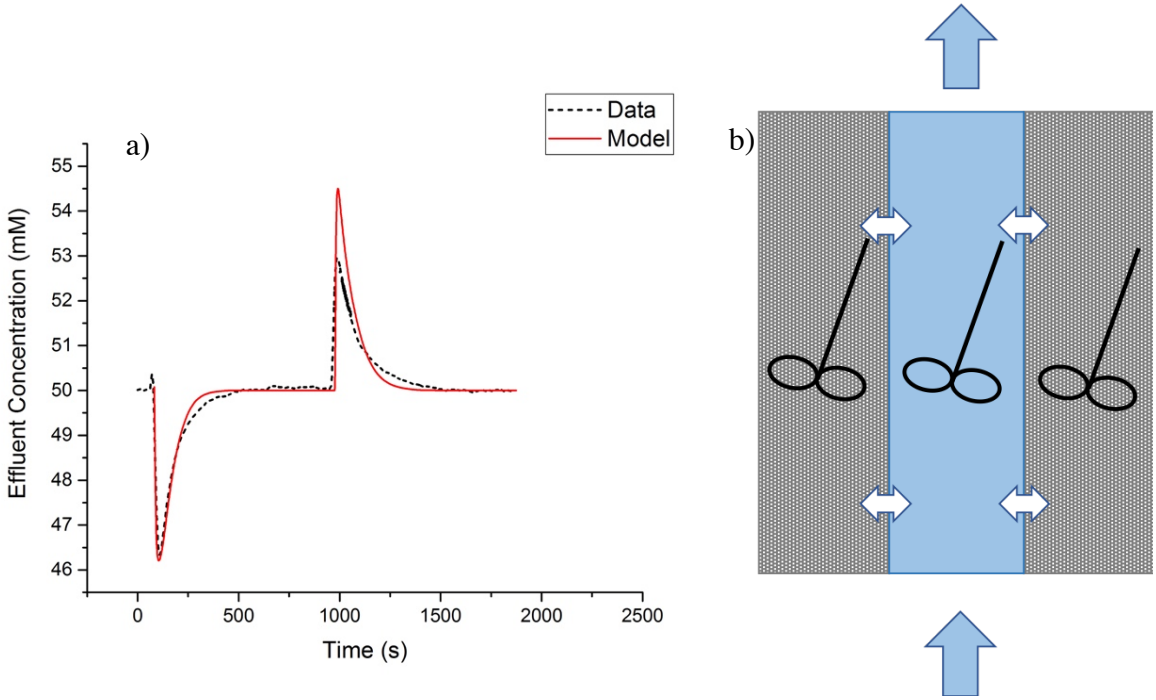

Figure 7. a) Comparison between the experimental data and the modeled curve for the AR-PVDF cell. It can be seen that the modeled system has faster adsorption/desorption kinetics. b) Schematic representation of the model used to depict behavior of the AR-PVDF cell.

4.1.1 Stern capacitance and transport resistance

The Stern layer capacitance is also an important value that needed to be fit. After trial and error, a value of 85 F/mL was obtained for the carbon under these conditions. The choice for such value comes from analyzing the effects of leakage current, height of co-ion repulsion peak, fluid dynamics, salt adsorption capacity and energy consumption in the modeled curve. The effects of leakage were studied, and it was observed that the system achieves equilibrium at a later stage with increasing leakage current. When looking at the equations, this effect is logical

since higher leakage implies a slower rate of change of the electronic charge and thus a slower change in the ionic charge density. However, the leakage current was determined from the experimental curves and this value was fixed throughout the simulations. Therefore, the diffusion timescale of the ions from the flow channel to the electrode was fitted, using an equivalent diffusion length that is 20% greater than that of the flow channel, adjusting in this way the resistance to ionic transport.

A co-ion repulsion peak similar to the one in the experiments could be observed across the simulations by varying Stern capacitance between 70 – 85 F/mL. However, with lower capacitance values, the SSA from the experiments was not possible to achieve. The number of sub-units in series was increased then, to observe the impact of fluid dynamics on the system. When increasing the number of stirred tanks in series, the fluid motion approaches the plug flow case, and thus, there is less mixing in the flow channel and the concentration is higher in each sub-domain. This is the reason why in Figure 8, we observe a lower concentration peak at a slightly earlier time. However, the fact that the curve expands further indicates that there was a greater amount of salt stored in the system. By fitting the resistance to the flow of current from the flow channel to the electrode, an SSA that differs only 8% from the experimental value was obtained.

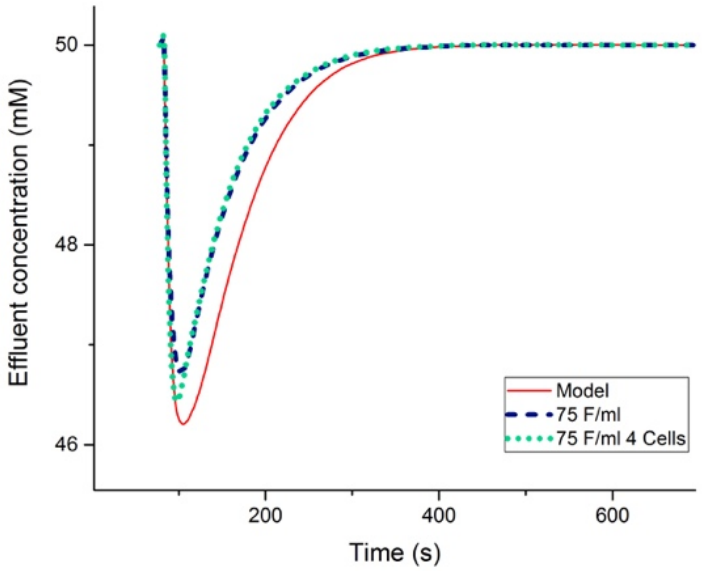

Figure 8. Comparison of modeled systems with different Stern capacitances. The curves reflect the impacts of fluid dynamics.

4.2 CS-CMC cell modeling

For the polysaccharide bound electrodes, a model employing CDI and MCDI cells in series was developed to verify the hypothesis that charged binders cover pores and introduce distributed ion-selectivity within the electrode macrostructure. The first thing to note about the results obtained experimentally is that there is a "hump" in the charging step below the influent concentration (Figure 3a), after which there is another decay in concentration, and finally the concentration increases linearly and does not return to the influent value. Although the MCDI/CDI hybrid system was not entirely accurate in depicting this exact behavior, results that may explain what has been observed experimentally for the binder were obtained.

4.2.1 Case study 2: CDI-MCDI in series

The CDI system that was fit for the AR-PVDF cell was taken as reference for the modeled CDI sub-units, meaning the parameters used for the modeling of this cell remain unchanged in each sub-unit. The first modification made to the model was to add an MCDI cell in series, whose surface area coverage corresponded to 7.5% of the total area, that is, it has been assumed that the binder influenced the current across an area that was equal to its percentage in the electrode formulation (Figure 9). For this first modification, the binder was assumed to possess a typical membrane's thickness, i.e. 150 um (Dykstra et al., 2017) and a fixed charge equal to CS's at pH 5. The measured leakage current from the experiments was also distributed proportionally to the percentage of material in the electrode, provided this value is taken analogous to the projected area. Figure 10a shows the result in comparison to the experimental binder curve obtained. What we observe, is a slightly faster decay in salt concentration when polarizing the electrodes than in the AR-PVDF system, which is certainly what we would expect for an IEM (Biesheuvel et al., 2011). The main distinctive feature of this system is that the co-ion repulsion peak disappears and that we achieve greater SSA, provided the greater area of the charging step curve. This result approaches what we would expect from an MCDI system (Biesheuvel et al., 2011), although we are not visualizing fully the improvements made to traditional CDI systems through the addition of membranes because the electrode surface area that exhibits MCDI behavior is only 7.5 % of the total. It is informative at this point, however, to observe how macropore and micropore concentrations change in each domain as a result of the membrane addition (Figures 10b & 10c). As expected, contrary to the CDI sub-unit, the membrane enhances salt removal by storing ions in the macropores, hence increasing the micropore concentration. The decay in the macropore concentration may be due to the low

charge density we are attributing to the membrane, and thus diffusive transport of ions back into the flow channel as a result of the concentration gradient is not completely hindered.

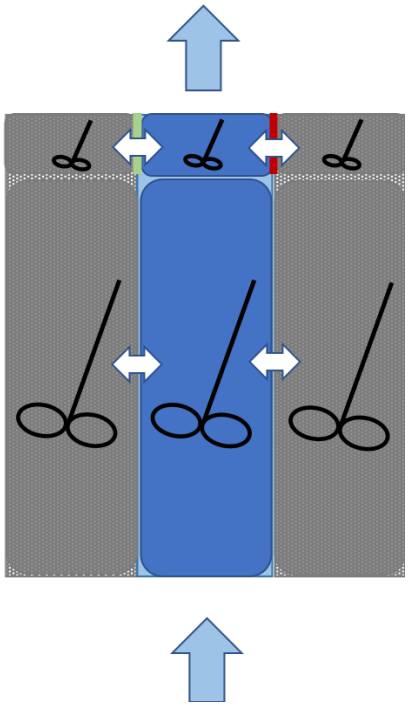

Figure 9. Schematic representation of the model used to depict behavior of the CS-CMC cell in case study 2. The green and red bars correspond to an anion-exchange membrane and a cation-exchange membrane, respectively.

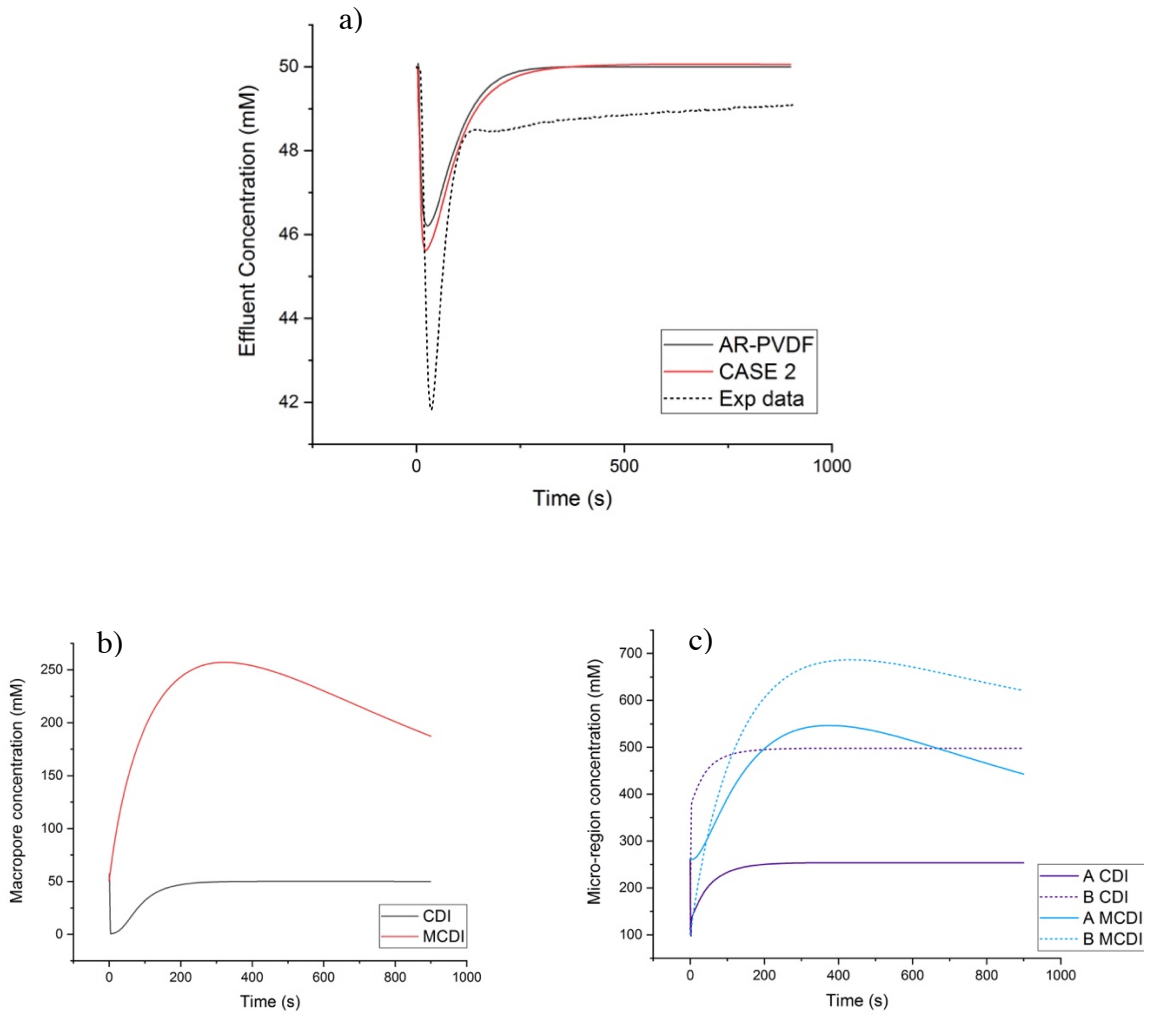

Figure 10. Case study 2: Experimental curve of the CS-CMC system in comparison to a system with a CDI and an MCDI in series, where the MCDI unit affected 7.5% of the total area, and the AR-PVDF cell. The MCDI parameters used for this simulation could be representative of commercial IEMs. Figures b and c correspond to the evolution of the concentration in the macro and micropore regions, where A means acidic and B basic, in each sub-unit.

4.2.2 Case study 3: CDI-MCDI in series with decreased membrane thickness

One thing to note about the experimental curve obtained is the "hump" observed when the cell is returning to equilibrium. This behavior may be attributed to rapid transport favored by the binder, which being much faster than ionic transport in the CDI cell dictates the overall behavior. To verify this hypothesis, the system described before was modified in such a way that

the thickness of the membrane was reduced to one tenth of its initial value, thus approaching the thickness of a polymer coating. Figure 11a shows the charging cycle under these conditions. What can be observed is that the macropore concentration in the MCDI cell returns to the influent value (Figure 11b), thus indicating that the concentration in the macropore region is so high that diffusive transport back into the flow channel is greater than the electromigration contribution, and the screening effect of the membrane's fixed charge is not sufficient to prevent transport motivated by the diffusion gradient. An indication that it is the membrane governing the cell's behavior is Figure 11a where it is seen that the effluent concentration is a lagged version of the membrane's flow channel volume, which makes sense considering the membrane is positioned at the end of the cell and its adsorption capacity is far greater than the CDI sub-unit's.

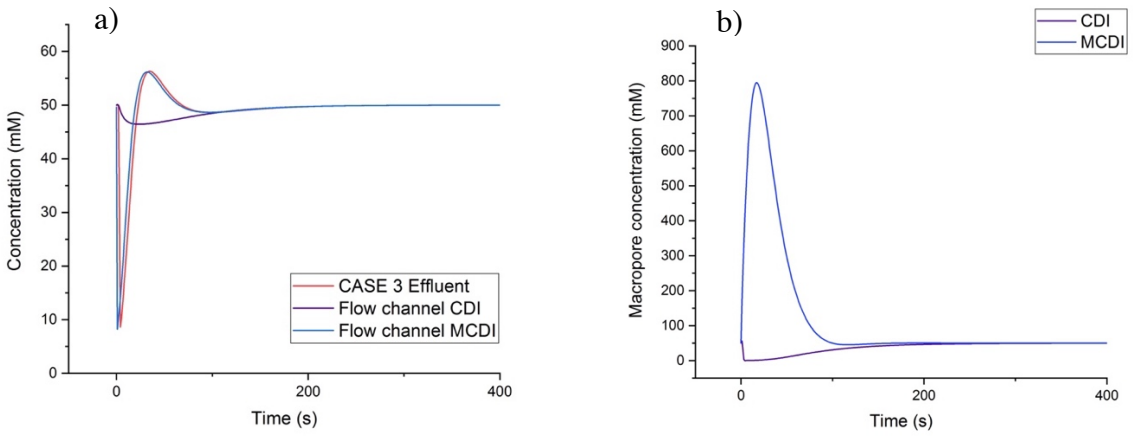

Figure 11. a) Charging cycle of a CDI-MCDI system, with the MCDI cell covering 7.5% of the total area, assuming a membrane thickness that is 10% out of the original value. The concentration in the flow channel of each sub-unit is taken as reference b) Macropore concentration in each sub-unit.

4.2.3 Case study 4: Distribution of the MCDI sub-units along the cell

An arrangement composed of 10 sub-units was used to assess the impacts of the heterogeneity of the electrode given that in reality, the binder is distributed in the electrode

matrix. The sub-units for this configuration followed the order: CDI, MCDI, CDI, CDI, CDI, CDI, MCDI, MCDI, MCDI, CDI, and a visual representation of these scheme can be found in Figure 12. This configuration was chosen under the assumption that given the higher concentration gradients that would result from MCDI cells desalinating faster downstream and CDI cells receiving higher influent concentrations and desalinating slower upstream, more mixing would occur and more diffusional limitations will appear. Figure 13 corroborates this assumption, since it can be seen that the effluent's concentration is higher than in Case 3 and there is a slight broadening of the curve. Still we observe an effluent concentration above the baseline, which is indicative of the existence of concentration gradients across the membrane which exceed the adsorption rate capabilities of the actual system.

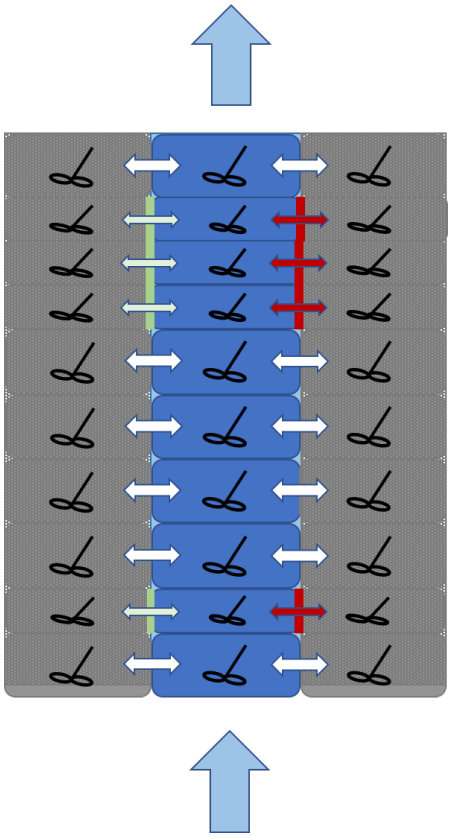

Figure 12. Schematic representation of the binder cell configuration implemented from cases 4 onwards, the only difference being the relative percentage of CDI to MCDI cells which is slightly lower for cases 5 & 6.

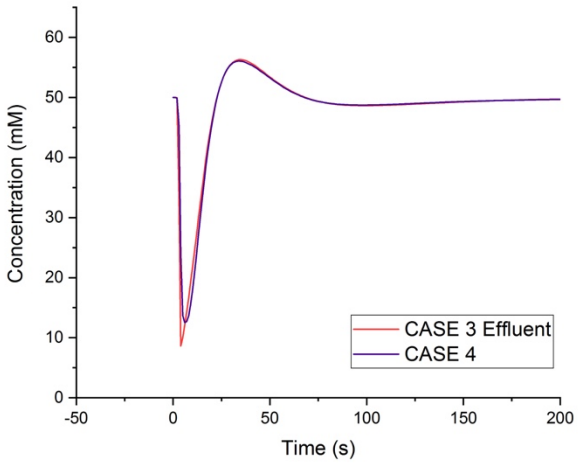

Figure 13. Comparison of the CDI-MCDI system from Case 3 and Case 4 which intercalates 10 CDI and MCDI sub-units.

4.2.4 Case study 5: Modification of the area covered by MCDI sub-units

The binder is technically not entirely exposed to the flow channel solution creating a selective barrier, but rather embedded in the electrode matrix which may result in the rapid transport effect observed in previous cases not to be as pronounced. Even if there is no screening of charge, the resulting transport processes will be a result of regions affected by the binder in immediate proximity with others that will exhibit typical CDI behavior. Hence, the surface area covered by the binder was decreased to 5% and the CDI coverage increased to 95%. Figure 14 shows how the behavior starts approximating the experimental data.

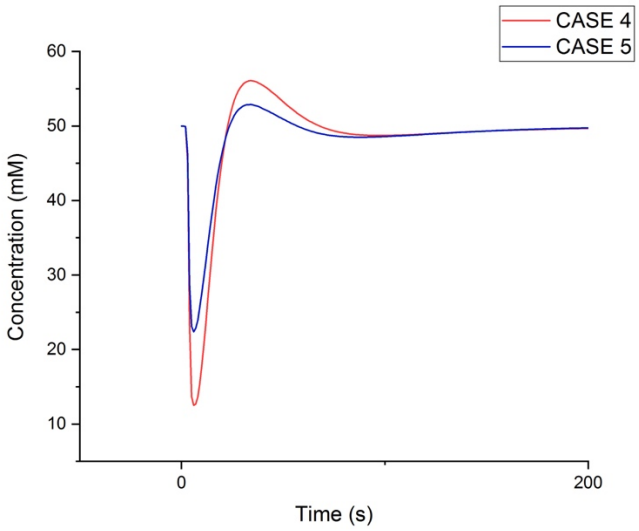

Figure 14. Comparison of cases 4 & 5. The difference in the curves is directly related to the distribution of MCDI units along the cell.

4.2.5 Case study 6: Reduction of the effective binder's fixed charge

It may be the case that given the interwoven nature of the electrode matrix some of the binder's charge is screened. Moreover, one of the initial assumptions of the model was that the carbon was oxidized, and thus the local pH in the binder's environment may not necessarily be equal to that of the influent. Thus, the fixed charge concentration was adjusted by reducing it to half its original value. The charging cycle results can be observed in Figure 15a & 15b. Using these parameters, a rapid increase in concentration is observed but the effluent concentration does not fall above the baseline, indicating that transport affected by the binder's fixed charge is slower, and so is the concentration gradient that develops across the selective interface. This reduced "induced capacity" by the binder results in the CDI sub-units having to desalinate a less concentrated flow channel and take in the salt released back by the MCDI units. The effluent finally reaches the baseline, indicating saturation of all the sub-units present in the cell, and loss of MCDI benefits. Proof of this behavior are the macropore concentration trends that Figures 16a

& 16b show, where a decline is observed in the CDI units concentration, whereas an initial increase and posterior decrease occurs in the MCDI subunits. Given that the micropore concentration follows the same trend (Figure 17), these are not ions that have been stored, but rather released back into the flow channel. This behavior suggests that after reaching a peak macropore concentration the MCDI subunits will start behaving as CDI desalination units. Nonetheless, it is important to distinguish between concentration and amount of salt stored. If we calculate the number of moles that were stored in the MCDI and CDI subunits, we observe the value is lower in the MCDI cell (Figure 18a). Although we cannot assure that the effective macropore concentration in the binder system is overall higher than what we observe, this conclusion points towards the fact that mixing inside the electrode may play a significant role in the overall desalination performance. Because the cells rather than being in series in the axial direction are also in series in the x-direction, the combination of effects may result in a higher SSA than that observed with the model (Figure 18b).

Moreover, we have assumed the percentage of binder in the composition should be somewhat representative of the covered pores proportion, but given the simplistic nature of our model the actual contribution of MCDI units may be higher. This parameter may be easily modified, but doing so implies changes in other features, such as the “hump” in the charging stage, and so we limit the analysis to the explanation of the main distinctive features of this modified system.

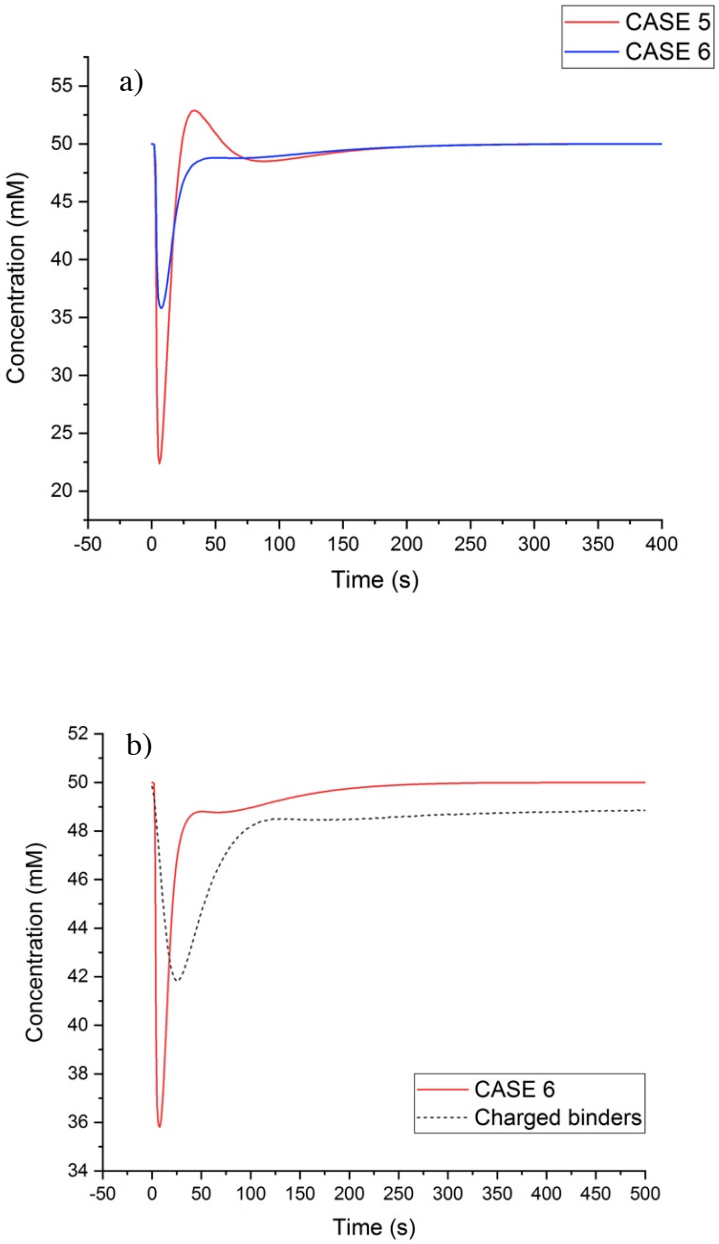

Figure 15. a) Comparison between the charging step in modeled systems 5 and 6. b) Comparison between Case 6 and the experimental data

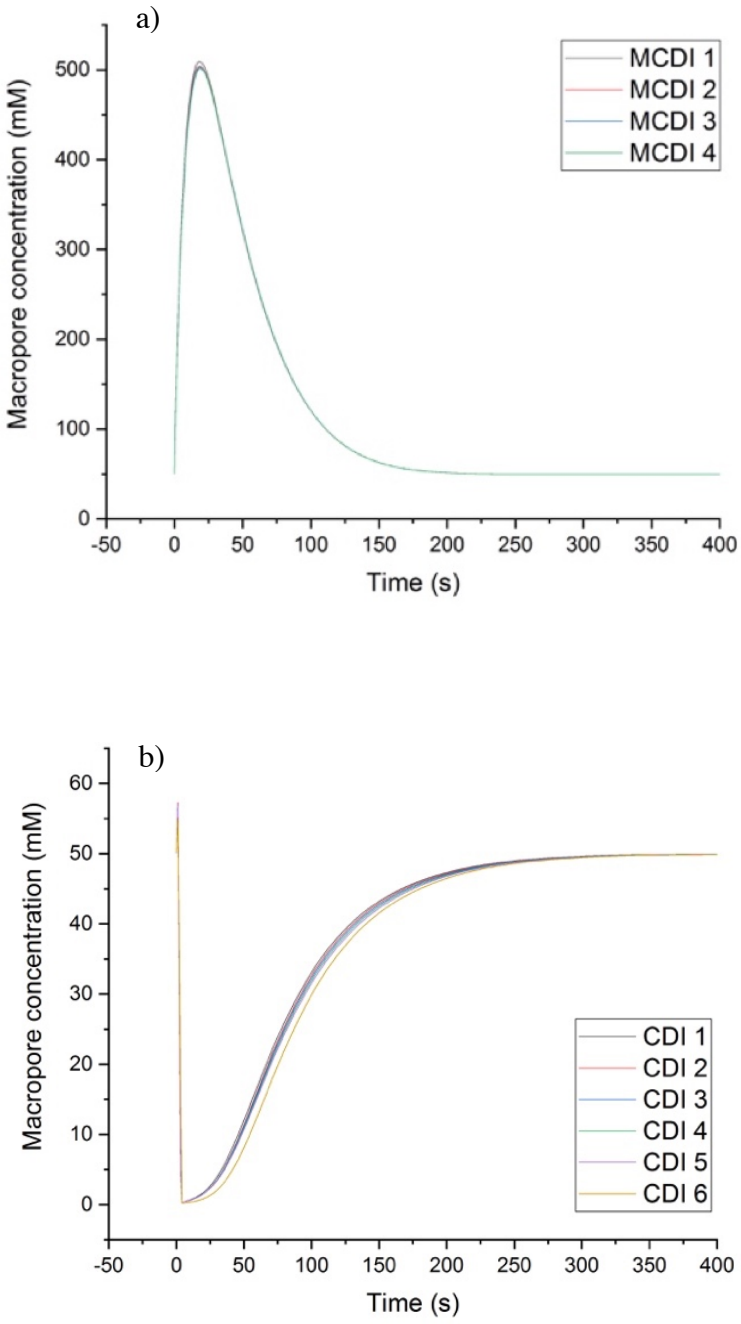

Figure 16. a) Evolution of macropore concentration in MCDI sub-units. b) Evolution of macropore concentration in CDI sub-units.

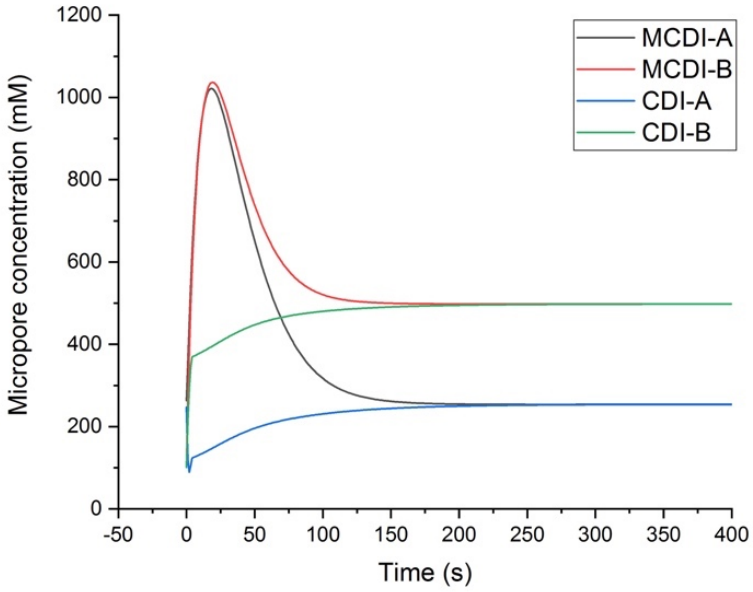

Figure 17. Evolution of micropore concentrations in MCDI and CDI sub-units. The behavior of the MCDI cells starts approaching that of CDI cells.

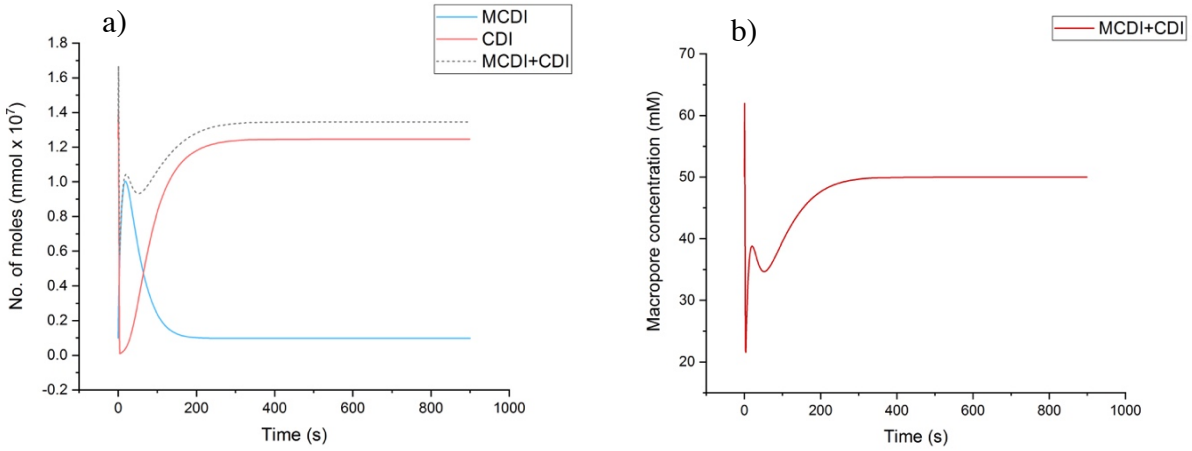

Figure 18. a) Macropore moles of salt for a CDI and an MCDI sub-unit. The dotted curve represents the addition of both CDI and MCDI macropore regions. b) Combined macropore concentration assuming the macrostructure is well-mixed.

4.2.6 Energy consumption

Introduction of the polysaccharide binders lowered the energy consumption of the system. The results obtained through the modeled system can be visualized in Figure 19. We observe how after the point where the MCDI units stop behaving as such, the total charge applied curve reaches the AR-PVDF system's. When breaking down the contribution to the total charge of MCDI and CDI sub-units we obtain the dotted lines in Figure 19. It is evident that the energy consumption of MCDI is significantly lower, thus pointing towards a different proportion of MCDI to CDI units. However, the results observed in the applied charge behavior, resemble what can be concluded from the ionic fluxes.

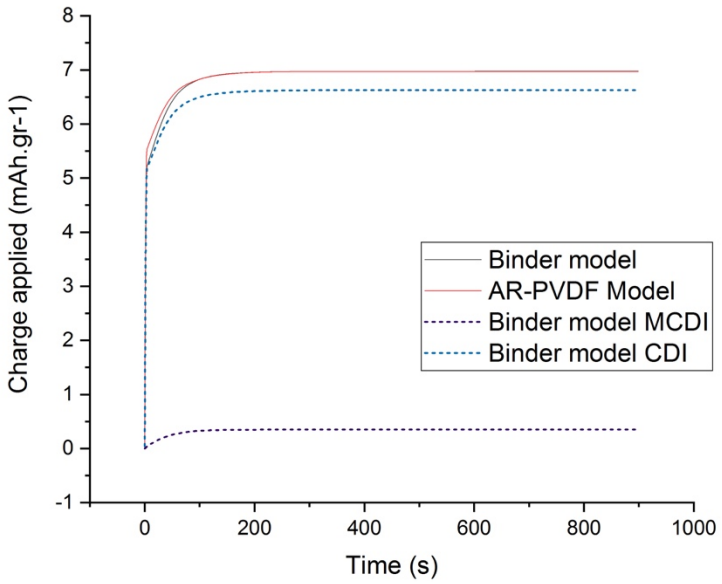

Figure 19. Applied electronic charge comparison between AR-PVDF and charged binders model, with a breakdown between the charge applied to the MCDI and CDI cells in the CS-CMC model.

4.2.7 Performance variation as a function of pH and determination of optimal pKa

It is known that pH affects the degree of ionization of chemical species. In the case of CS, a higher pH than 6.3 implies that there will be a predominance of its deprotonated form.

Contrary to what is observed experimentally with the binder, the model interprets that the fixed charge in the MCDI unit is almost null, and so the behavior approaches a CDI cell. This is also in alignment with the assumption that both IEM's are symmetric, since CMC preserves its fixed charge while CS becomes progressively less positive. Therefore, the model may predict greater losses in desalination performance than the actual system does (Figure 20). Moreover, ions in the effluent need to diffuse through the electrode matrix and there might not be such a direct relationship as the one predicted by the equilibrium in terms of the degree of ionization of the species. It is also important to highlight that pH changes inside the electrode are not being considered and there might be other factors contributing to changes in local pH. Figure 21a shows how the simulated curve starts to resemble the AR-PVDF curve (Figure 7a), which is in agreement with the fact that the lower the fixed charge in the MCDI sub-units the greater the similarities with CDI behavior.

Finally, the curve from Case 7 was taken as a reference to assess the ideal pKa of the binder species to be immune to pH fluctuations. After trial and error, the curve at pH 9 using a pKa value of 10 was practically identical to the curve obtained using CS's pKa at pH 5 (Figure 21b).

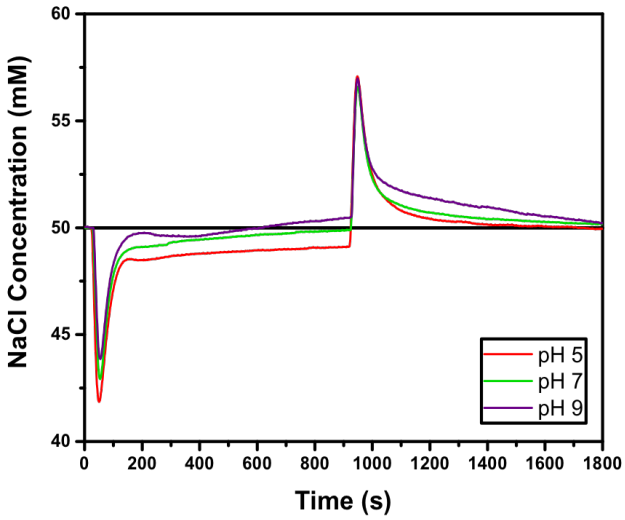

Figure 20. (Kim et al., in prep.) Desalination curves as a function of pH for the CS-CMC system. A decline in SSA is observed when deviating further from Chitosan's pKa of 6.3.

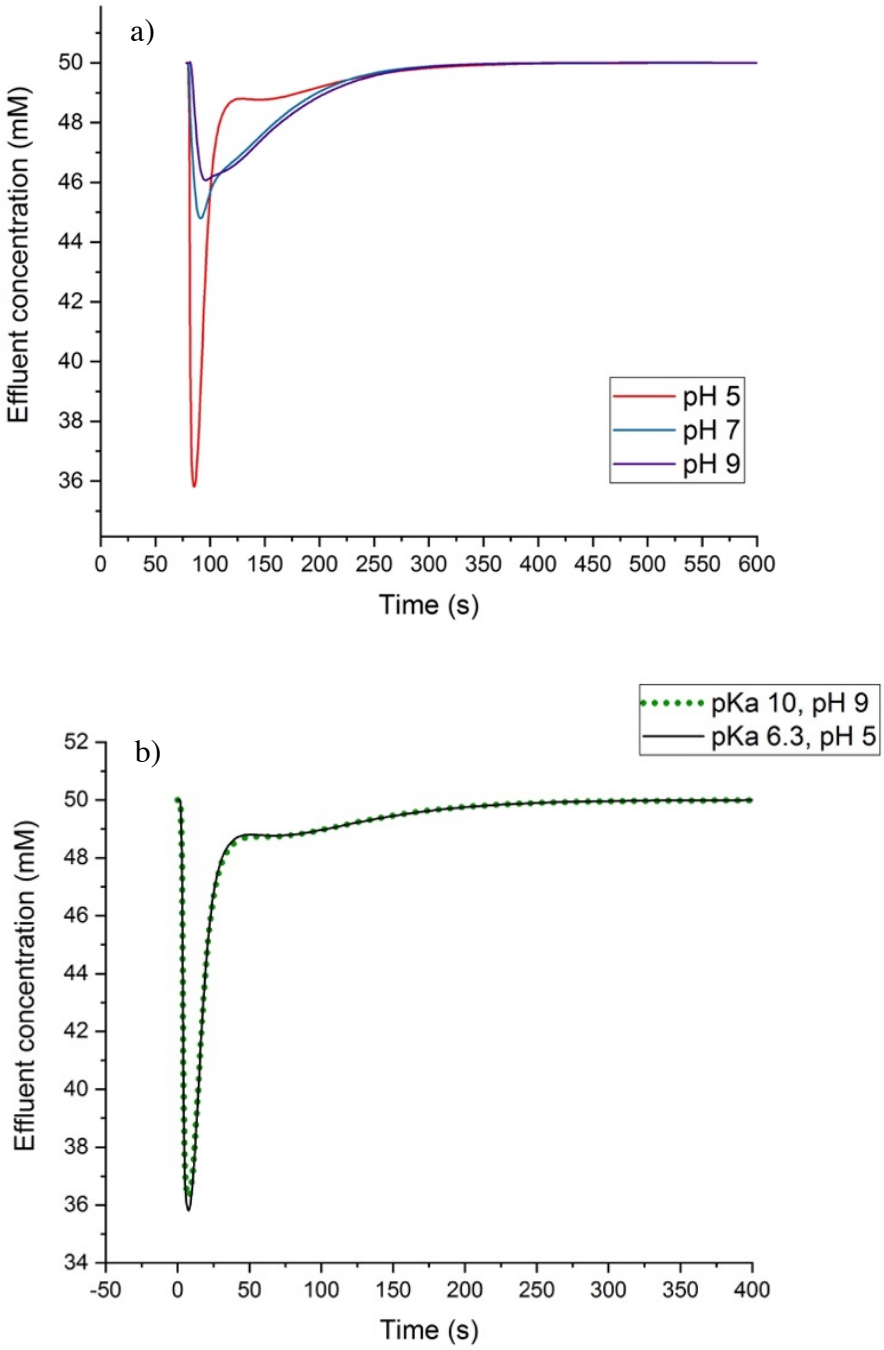

Figure 21. a) Comparison of the modeled system's performance at different pH. The loss of selectivity when the pH is higher is clearly observed. b) Charging step comparison between Case 7 and the same cell configuration assuming a binder pKa of 10 and pH 9.

CHAPTER 5

CONCLUSIONS AND RECOMMENDATIONS

It was possible to capture the distinctive features exhibited by CDI cells using electrodes with polysaccharide binders, although the model did not fit the experimental data. As for the AR-PVDF system, a co-ion repulsion peak, which is normally neglected in published CDI models, was simulated. The effectiveness of fixed chemical charge in getting rid of this undesired behavior was also corroborated.

The development of this model shed light on the complexities that studying transport at the micro/nano scale level may embed. While we were not able to directly prove the electrosorption capacity of macropores, we did observe interesting behaviors in ionic transport induced by the introduction of fixed charge, such as rapid transport across thin interfaces affected by high concentration gradients. For this system to be thoroughly represented, it may seem accurate to include mixing inside the electrode structure. It would also be wise to solve for the mass balance of each species individually, to fully realize the impact of both anodic and cathodic binders in the cell, as well as pH. This study exceeded the scope of the present work. However, the findings suggest that measuring desalination performance in a modified CDI unit with known macrostructure and fixed charge symmetry may reveal interesting ionic transport mechanisms which are up to date not fully understood.

CHAPTER 6

REFERENCES

Ahualli, S., Iglesias, G. R., Fernández, M. M., Jiménez, M. L., & Delgado, Á. V. (2017). Use of Soft Electrodes in Capacitive Deionization of Solutions. Environmental Science & Technology, 51(9), 5326–5333. https://doi.org/10.1021/acs.est.6b06181

Al-Karaghouli, A., & Kazmerski, L. L. (2013). Energy consumption and water production cost of conventional and renewable-energy-powered desalination processes. Renewable and Sustainable Energy Reviews, 24, 343-356. https://doi.org/10.1016/j.rser.2012.12.064

Avraham, E., Bouhadana, Y., Soffer, A., & Aurbach, D. (2009). Limitation of Charge Efficiency in Capacitive Deionization I. On the Behavior of Single Activated Carbon. Journal of The Electrochemical Society, 156(6), P95–P99. https://doi.org/10.1149/1.3115463

Bard, A. J., Faulkner, L. R., Electrochemical Methods: Fundamentals and Applications, 2nd Edition. John Wiley & Sons, 2000.

Biesheuvel, P.M. and van der Wal, A. (2010). Membrane capacitive deionization. Journal of Membrane Science, Volume 346, Issue 2, Pages 256-262, https://doi.org/10.1016/j.memsci.2009.09.043.

Biesheuvel, P. M., Zhao, R., Porada, S., & Van der Wal, A. (2011). Theory of membrane capacitive deionization including the effect of the electrode pore space. Journal of Colloid and Interface Science, 360(1), 239-248. https://doi.org/10.1016/j.jcis.2011.04.049

Biesheuvel, P. M. (2015). Activated carbon is an electron-conducting amphoteric ion adsorbent. arXiv:1509.06354 [Physics]. Retrieved from http://arxiv.org/abs/1509.06354

Biesheuvel, P.M., Hamelers, H.V.M., Suss, M.E. (2015). Theory of Water Desalination by Porous Electrodes with Immobile Chemical Charge. Colloids and Interface Science Communications, Volume 9, 1-5, https://doi.org/10.1016/j.colcom.2015.12.001.

Boehm, H.P. (1994). Some aspects of the surface chemistry of carbon blacks and other carbons, Carbon, Volume 32, Issue 5, Pages 759-769, https://doi.org/10.1016/0008-6223(94)90031-0.

Chai, L., Qu, Q., Zhang, L., Shen, M., Zhang, L., & Zheng, H. (2013). Chitosan, a new and environmental benign electrode binder for use with graphite anode in lithium-ion batteries. Electrochimica Acta, 105, 378-383. https://doi.org/10.1016/j.electacta.2013.05.009

Długołęcki, P., & van der Wal, A. (2013). Energy Recovery in Membrane Capacitive Deionization. Environmental Science & Technology, 47(9), 4904–4910. https://doi.org/10.1021/es3053202

Dykstra, J. E., Keesman, K. J., Biesheuvel, P. M., & van der Wal, A. (2017). Theory of pH changes in water desalination by capacitive deionization. Water Research, 119(Supplement C), 178–186. https://doi.org/10.1016/j.watres.2017.04.039

Elimelech, M., & Phillip, W. A. (2011). The Future of Seawater Desalination: Energy, Technology, and the Environment. Science, 333(6043), 712–717. https://doi.org/10.1126/science.1200488

Fritzmann, C., Löwenberg, J., Wintgens, T., & Melin, T. (2007). State-of-the-art of reverse osmosis desalination. Desalination, 216(1-3), 1-76. https://doi.org/10.1016/j.desal.2006.12.009

Gabitto, J., & Tsouris, C. (2016). Modeling the Capacitive Deionization Process in Dual-Porosity Electrodes. Transport in Porous Media, 113(1), 173–205. https://doi.org/10.1007/s11242-016-0688-9

Gao, X., Omosebi, A., Landon, J., & Liu, K. (2015). Surface charge enhanced carbon electrodes for stable and efficient capacitive deionization using inverted adsorption–desorption behavior. Energy & Environmental Science, 8(3), 897–909. https://doi.org/10.1039/C4EE03172

Gao, X., Porada, S., Omosebi, A., Liu, K.-L., Biesheuvel, P.M., Landon, J. (2016). Complementary surface charge for enhanced capacitive deionization, Water Research, Volume 92, 275-282, https://doi.org/10.1016/j.watres.2016.01.048.

Ghaffour, N., Missimer, T. M., & Amy, G. L. (2013). Technical review and evaluation of the economics of water desalination: current and future challenges for better water supply sustainability. Desalination, 309, 197-207. https://doi.org/10.1016/j.desal.2012.10.015

Greenlee, Lauren F., Lawler, Desmond F., Freeman, Benny D., Marrot, Benoit, Moulin, Philippe (2009). Reverse osmosis desalination: Water sources, technology, and today's challenges. Water Research, Volume 43, Issue 9, 2317-2348, https://doi.org/10.1016/j.watres.2009.03.010.

Guyes, E. N., Shocron, A. N., Simanovski, A., Biesheuvel, P. M., & Suss, M. E. (2017). A one-dimensional model for water desalination by flow-through electrode capacitive deionization. Desalination, 415(Supplement C), 8–13. https://doi.org/10.1016/j.desal.2017.03.013

Hassanvand, A., Chen, G. Q., Webley, P. A., & Kentish, S. E. (2017). Improvement of MCDI operation and design through experiment and modelling: Regeneration with brine and

optimum residence time. Desalination, 417, 36–51. https://doi.org/10.1016/j.desal.2017.05.004

Holubowitch, N., Omosebi, A., Gao, X., Landon, J., & Liu, K. (2017). Quasi-Steady-State Polarization Reveals the Interplay of Capacitive and Faradaic Processes in Capacitive Deionization. ChemElectroChem, 4(9), 2404–2413. https://doi.org/10.1002/celc.201700082

Hussey, K., & Pittock, J. (2012). The energy–water nexus: Managing the links between energy and water for a sustainable future. Ecology and Society, 17(1). http://dx.doi.org/10.5751/ES-04641-170131

Jain, A., Kim, J., Owoseni, O. M., Weathers, C., Cana, D., Zuo, K., … Verduzco, R. (2018). Aqueous-Processed, High-Capacity Electrodes for Membrane Capacitive Deionization. Environmental Science & Technology. https://doi.org/10.1021/acs.est.7b05874

Jeon, B. G., No, H. C., & Lee, J. I. (2011). Development of a two-dimensional coupled-implicit numerical tool for the optimal design of CDI electrodes. Desalination, 274(1–3), 226–236. https://doi.org/10.1016/j.desal.2011.02.021

Jeon, S., Park, H., Yeo, J., Yang, S., Hee Cho, C., Hee Han, M., & Kook Kim, D. (2013). Desalination via a new membrane capacitive deionization process utilizing flow-electrodes. Energy & Environmental Science, 6(5), 1471–1475. https://doi.org/10.1039/C3EE24443A

Jeon, S., Yeo, J., Yang, S., Choi, J., & Kook Kim, D. (2014). Ion storage and energy recovery of a flow-electrode capacitive deionization process. Journal of Materials Chemistry A, 2(18), 6378–6383. https://doi.org/10.1039/C4TA00377B

Kang, J., Kim, T., Jo, K., Yoon, J. (2014). Comparison of salt adsorption capacity and energy consumption between constant current and constant voltage operation in capacitive deionization. Desalination, Volume 352, 52-57, https://doi.org/10.1016/j.desal.2014.08.009.

Karabelas, A. J., Koutsou, C. P., Kostoglou, M., & Sioutopoulos, D. C. (2017). Analysis of specific energy consumption in reverse osmosis desalination processes. Desalination. https://doi.org/10.1016/j.desal.2017.04.006

Kim, J. S., & Choi, J. H. (2010). Fabrication and characterization of a carbon electrode coated with cation-exchange polymer for the membrane capacitive deionization applications. Journal of membrane science, 355(1-2), 85-90. https://doi.org/10.1016/j.memsci.2010.03.010

Kim, T., Dykstra, J. E., Porada, S., Van Der Wal, A., Yoon, J., & Biesheuvel, P. M. (2015). Enhanced charge efficiency and reduced energy use in capacitive deionization by increasing the discharge voltage. Journal of colloid and interface science, 446, 317-326. https://doi.org/10.1016/j.jcis.2014.08.041

Lee, J. B., Park, K. K., Eum, H. M., & Lee, C. W. (2006). Desalination of a thermal power plant wastewater by membrane capacitive deionization. Desalination, 196(1-3), 125-134. https://doi.org/10.1016/j.desal.2006.01.011

Lee, J. Y., Seo, S. J., Yun, S. H., & Moon, S. H. (2011). Preparation of ion exchanger layered electrodes for advanced membrane capacitive deionization (MCDI). Water research, 45(17), 5375-5380. https://doi.org/10.1016/j.watres.2011.06.028

Li, J., Lewis, R. B., & Dahn, J. R. (2007). Sodium Carboxymethyl Cellulose A Potential Binder for Si Negative Electrodes for Li-Ion Batteries. Electrochemical and Solid-State Letters, 10(2), A17–A20. https://doi.org/10.1149/1.2398725

Li Zhang, L., & S. Zhao, X. (2009). Carbon-based materials as supercapacitor electrodes. Chemical Society Reviews, 38(9), 2520–2531. https://doi.org/10.1039/B813846J

Li, N., An, J., Wang, X., Wang, H., Lu, L., & Ren, Z. J. (2017). Resin-enhanced rolling activated carbon electrode for efficient capacitive deionization. Desalination, 419(Supplement C), 20–28. https://doi.org/10.1016/j.desal.2017.05.035

Li, Y., Shen, J., Li, J., Sun, X., Shen, J., Han, W., & Wang, L. (2017). A protic salt-derived porous carbon for efficient capacitive deionization: Balance between porous structure and chemical composition. Carbon, 116, 21–32. https://doi.org/10.1016/j.carbon.2017.01.084

Liu, J., Geise, G. M., Luo, X., Hou, H., Zhang, F., Feng, Y., … Logan, B. E. (2014). Patterned ion exchange membranes for improved power production in microbial reverse-electrodialysis cells. Journal of Power Sources, 271(Supplement C), 437–443. https://doi.org/10.1016/j.jpowsour.2014.08.026

McGinnis, R. L., & Elimelech, M. (2008). Global Challenges in Energy and Water Supply: The Promise of Engineered Osmosis. Environmental Science & Technology, 42(23), 8625–8629. https://doi.org/10.1021/es800812m

Newman, J., Thomas-Alyea, K. E. (2004). Electrochemical Systems. Third Edition. John Wiley & Sons, Inc.

Omosebi, A., Gao, X., Landon, J., & Liu, K. (2014). Asymmetric electrode configuration for enhanced membrane capacitive deionization. ACS Applied Materials and Interfaces, 6(15), 12640–12649. https://doi.org/10.1021/am5026209

Oren, Y. (2008). Capacitive deionization (CDI) for desalination and water treatment — past, present and future (a review). Desalination, Volume 228, Issues 1–3, 10-29, https://doi.org/10.1016/j.desal.2007.08.005.

Park, B. H., & Choi, J. H. (2010). Improvement in the capacitance of a carbon electrode prepared using water-soluble polymer binder for a capacitive deionization application. Electrochimica Acta, 55(8), 2888-2893. https://doi.org/10.1016/j.electacta.2009.12.084

Porada, S., Bryjak, M., van der Wal, A., & Biesheuvel, P. M. (2012). Effect of electrode thickness variation on operation of capacitive deionization. Electrochimica Acta, 75, 148–156. https://doi.org/10.1016/j.electacta.2012.04.083

Porada, S., Weinstein, L., Dash, R., van der Wal, A., Bryjak, M., Gogotsi, Y., & Biesheuvel, P. M. (2012). Water Desalination Using Capacitive Deionization with Microporous Carbon Electrodes. ACS Applied Materials & Interfaces, 4(3), 1194–1199. https://doi.org/10.1021/am201683j

Porada, S., Borchardt, L., Oschatz, M., Bryjak, M., Atchison, J. S., Keesman, K. J., … Presser, V. (2013). Direct prediction of the desalination performance of porous carbon electrodes for capacitive deionization. Energy & Environmental Science, 6(12), 3700. https://doi.org/10.1039/c3ee42209g

S. Porada, R. Zhao, A. van der Wal, V. Presser, P.M. Biesheuvel (2013). Review on the science and technology of water desalination by capacitive deionization, Progress in Materials Science, Volume 58, Issue 8, Pages 1388-1442, https://doi.org/10.1016/j.pmatsci.2013.03.005.

Qu, Y., Campbell, P. G., Gu, L., Knipe, J. M., Dzenitis, E., Santiago, J. G., Stadermann, M. (2016). Energy consumption analysis of constant voltage and constant current operations in capacitive deionization. Desalination, Volume 400, 18-24, https://doi.org/10.1016/j.desal.2016.09.014.

Sarkar, S., SenGupta, A. K., & Prakash, P. (2010). The Donnan Membrane Principle: Opportunities for Sustainable Engineered Processes and Materials. Environmental Science & Technology, 44(4), 1161–1166. https://doi.org/10.1021/es9024029

Scanlon, B. R., Duncan, I., & Reedy, R. C. (2013). Drought and the water–energy nexus in Texas. Environmental Research Letters, 8(4), 45033. https://doi.org/10.1088/1748-9326/8/4/045033

Semiat, R. (2008). Energy Issues in Desalination Processes. Environmental Science & Technology, 42(22), 8193–8201. https://doi.org/10.1021/es801330u

Service, R. F. (2006). Desalination Freshens Up. Science, 313(5790), 1088–1090. https://doi.org/10.1126/science.313.5790.1088

Strathmann, H. (2004). Assessment of electrodialysis water desalination process costs. In Proceedings of the International Conference on Desalination Costing, Limassol, Cyprus (pp. 32-54).

Strathmann, H. (2010). Electrodialysis, a mature technology with a multitude of new applications. Desalination, 264(3), 268-288. https://doi.org/10.1016/j.desal.2010.04.069

Suss, M. E., Porada, S., Sun, X., Biesheuvel, P. M., Yoon, J., & Presser, V. (2015). Water desalination via capacitive deionization: what is it and what can we expect from it? Energy & Environmental Science, 8(8), 2296–2319. https://doi.org/10.1039/C5EE00519A

Tanaka, Y. (2011). Ion-Exchange Membrane Electrodialysis for Saline Water Desalination and Its Application to Seawater Concentration. Industrial & Engineering Chemistry Research, 50(12), 7494–7503. https://doi.org/10.1021/ie102386d

Tang, W., He, D., Zhang, C., Kovalsky, P., & Waite, T. D. (2017). Comparison of Faradaic reactions in capacitive deionization (CDI) and membrane capacitive deionization (MCDI) water treatment processes. Water research, 120, 229-237. https://doi.org/10.1016/j.watres.2017.05.009

Tedesco, M., Hamelers, H.V.M., Biesheuvel, P.M. (2016). Nernst-Planck transport theory for (reverse) electrodialysis: I. Effect of co-ion transport through the membranes. Journal of Membrane Science, Volume 510, 370-381, https://doi.org/10.1016/j.memsci.2016.03.012.

Tian, G., Liu, L., Meng, Q., & Cao, B. (2014). Preparation and characterization of cross-linked quaternised polyvinyl alcohol membrane/activated carbon composite electrode for membrane capacitive deionization. Desalination, 354, 107-115. https://doi.org/10.1016/j.desal.2014.09.024

Tidwell, V. C. (2016). Energy-Water Nexus: Challenges and Opportunities (No. SAND2016-1883C). Sandia National Laboratories (SNL-NM), Albuquerque, NM (United States).

Van der Bruggen, B., Vandecasteele, C. (2002). Distillation vs. membrane filtration: overview of process evolutions in seawater desalination, Desalination, Volume 143, Issue 3, 207-218, https://doi.org/10.1016/S0011-9164(02)00259-X.

Veerman, J., & Vermaas, D. A. (2016). 4 - Reverse electrodialysis: Fundamentals. In A. Cipollina & G. Micale (Eds.), Sustainable Energy from Salinity Gradients (pp. 77–133). Woodhead Publishing. https://doi.org/10.1016/B978-0-08-100312-1.00004-3

Xu, T. (2005). Ion exchange membranes: State of their development and perspective, Journal of Membrane Science, Volume 263, Issues 1–2, Pages 1-29, https://doi.org/10.1016/j.memsci.2005.05.002.

Yan, T., Xu, B., Zhang, J., Shi, L., & Zhang, D. (2018). Ion-selective asymmetric carbon electrodes for enhanced capacitive deionization. RSC Advances, 8(5), 2490–2497. https://doi.org/10.1039/C7RA10443J

Zhang, H., Liu, B., Wu, M. S., Zhou, K., & Law, A. W. K. (2017). Transport of salty water through graphene bilayer in an electric field: A molecular dynamics study. Computational Materials Science, 131, 100-107. https://doi.org/10.1016/j.commatsci.2017.01.039

Zhao, R., M. Biesheuvel, P., & Wal, A. van der. (2012). Energy consumption and constant current operation in membrane capacitive deionization. Energy & Environmental Science, 5(11), 9520–9527. https://doi.org/10.1039/C2EE21737F

Zhao, Y., Wang, Y., Wang, R., Wu, Y., Xu, S., & Wang, J. (2013). Performance comparison and energy consumption analysis of capacitive deionization and membrane capacitive deionization processes. Desalination, 324, 127-133. https://doi.org/10.1016/j.desal.2013.06.009

Zhao, S., Yan, T., Wang, H., Zhang, J., Shi, L., & Zhang, D. (2016). Creating 3D Hierarchical Carbon Architectures with Micro-, Meso-, and Macropores via a Simple Self-Blowing Strategy for a Flow-through Deionization Capacitor. ACS Applied Materials & Interfaces, 8(28), 18027–18035. https://doi.org/10.1021/acsami.6b03704